

DISEASES AND DISORDERS

Extracellular serine empowers epidermal proliferation and psoriasis-like symptoms

Angela Cappello^{1,2}, Mara Mancini², Stefania Madonna², Serena Rinaldo³, Alessio Paone³, Claudia Scarponi², Antonio Belardo⁴, Lello Zolla⁴, Alessandro Zuccotti², Emanuele Panatta¹, Sabatino Pallotta², Margherita Annicchiarico-Petruzzelli², Cristina Albanesi², Francesca Cutruzzola³, Lu Wang⁵, Wei Jia⁵, Gerry Melino¹, Eleonora Candi^{1,2*}

The contribution of nutrient availability to control epidermal cell proliferation, inflammation, and hyperproliferative diseases remains unknown. Here, we studied extracellular serine and serine/glycine metabolism using human keratinocytes, human skin biopsies, and a mouse model of psoriasis-like disease. We focused on a metabolic enzyme, serine hydroxymethyltransferase (SHMT), that converts serine into glycine and tetrahydrofolate-bound one-carbon units to support cell growth. We found that keratinocytes are both serine and glycine auxotrophs. Metabolomic profiling and hypoxanthine supplementation indicated that SHMT silencing/inhibition reduced cell growth through purine depletion, leading to nucleotide loss. In addition, topical application of an SHMT inhibitor suppressed both keratinocyte proliferation and inflammation in the imiquimod model and resulted in a decrease in psoriasis-associated gene expression. In conclusion, our study highlights SHMT2 activity and serine/glycine availability as an important metabolic hub controlling both keratinocyte proliferation and inflammatory cell expansion in psoriasis and holds promise for additional approaches to treat skin diseases.

INTRODUCTION

The epidermis is a multilayer epithelium that continuously renews during an organism's life span. The maintenance of tissue in adult life is a result of somatic stem cells in the basal layer that control cell turnover, thus balancing proliferation with terminal differentiation (1, 2). It is becoming clear that cellular metabolites, including amino acids, through different mechanisms, involving both the control of anabolic reactions and epigenetic changes, are crucial determinants for somatic stem cell maintenance and differentiation (3–7). The nonessential amino acid serine is required for important anabolic processes in cellular metabolism, including nucleotides, reduced form of nicotinamide adenine dinucleotide phosphate (NADPH), and glutathione (GSH) synthesis. At the cellular level, serine can be imported from the extracellular environment; alternatively, it can be synthesized from glucose via the phosphoserine pathway. How serine is accessed for cellular biosynthesis varies among proliferating cell types.

The serine hydroxymethyltransferase (SHMT) enzyme, which converts serine and tetrahydrofolate (THF) into glycine and 5,10-methylenetetrahydrofolate (5,10-CH₂-THF), is key to fueling the one-carbon metabolism, sustaining the biosynthesis of nucleotide precursors and NADPH (8–10). In addition, the hydroxymethyl group cleaved from serine enters the THF cycle, providing a substantial source of one-carbon units for methylation reactions (11). In human cells, two genes encode three SHMT isoforms, mitochondrial SHMT2 and the cytosolic SHMT1 and SHMT2α isoforms. The mitochondrial SHMT2 enzyme is mainly involved in the

production of glycine and one-carbon units consumed in the synthesis of purines, thymidine monophosphate, NADPH, and GSH. The cytosolic isoforms SHMT1 and SHMT2α, depending on the metabolic requirements, can switch the direction of the reactions they catalyze, resulting in greater cellular adaptability to metabolic needs (12, 13). Both SHMT1 and SHMT2α undergo sumo-dependent translocation into the nucleus, where they form a ternary complex with other enzymes to provide thymine to DNA replication forks (14–16).

Proliferating cells are highly dependent on extracellular serine to support bioenergetic and anabolic reactions (8, 17, 18). Previous works with lymphocytes and lung epithelial cells demonstrated that serine-dependent one-carbon units are required for nucleotide synthesis to support proliferation (9, 19). Tumors, for instance, often overexpress one or more SHMT isoforms, while others increase de novo serine biosynthesis from glucose to drive growth (10, 20–22). Extracellular serine has been recently described as a crucial determinant of murine epidermal stem cell fate and skin tumor initiation in high-turnover tissues such as the epidermis (3). How keratinocytes used extracellular serine and glycine is currently unknown.

Here, we address the role of serine metabolism and SHMT2 in human keratinocytes. We report that serine and glycine are essential metabolites for optimal keratinocyte growth. Keratinocytes cultured without exogenous serine/glycine or with endogenous SHMT isoforms with suboptimal expression and activity show decreased proliferation and reduced synthesis of bioenergetic metabolites. Psoriasis is a common chronic skin disorder characterized by keratinocyte hyperproliferation with altered differentiation and inflammation. It remains unclear whether the first events that initiate psoriasis development occur in keratinocytes or in inflammatory cells. Our data implicate serine/glycine availability and serine catabolism as intrinsic regulators of both keratinocyte proliferation and inflammatory cell expansion, suggesting serine acquisition and

Copyright © 2022
The Authors, some
rights reserved;
exclusive licensee
American Association
for the Advancement
of Science. No claim to
original U.S. Government
Works. Distributed
under a Creative
Commons Attribution
NonCommercial
License 4.0 (CC BY-NC).

Downloaded from <https://www.science.org> on January 29, 2023

¹Department of Experimental Medicine, University of Rome "Tor Vergata", 00133 Rome, Italy. ²Istituto Dermatologico dell'Immacolata, IDI-IRCCS, 00167 Rome, Italy. ³Department of Biochemical Sciences A.Rossi Fanelli, Sapienza University of Rome, 00185 Rome, Italy. ⁴Agriculture and Forest Sciences (DAFNE), University of Tuscia, 01100 Viterbo, Italy. ⁵Chinese Medicine and Systems Biology/School of Chinese Medicine, Hong Kong Baptist University, Kowloon Tong, Hong Kong. *Corresponding author. Email: candi@uniroma2.it

serine metabolism as potential therapeutic targets for psoriasis. These findings reveal that nutrients control keratinocyte growth, thus defining that the basal line of keratinocyte metabolism is critical to design possible additional actionable therapies and approaches to treating skin disorders.

RESULTS

Extracellular serine and glycine are required to sustain keratinocyte proliferation and differentiation

To understand the role of extracellular serine utilization in keratinocytes, we analyzed the consequences of serine withdrawal from cultures of primary human keratinocytes. To minimize the effects arising from these cells converting glycine to serine under starvation conditions, we also removed glycine from the culture medium. We observed a significant reduction in keratinocyte proliferation upon serine (Ser), glycine (Gly), and Ser/Gly starvation (Fig. 1A), indicating that human keratinocytes rely on these amino acids to sustain cellular growth. The reduction in keratinocyte proliferation upon Ser/Gly deprivation was unexpected, given that both can be synthesized de novo. The block of de novo serine biosynthesis by chemical inhibition of phosphoglycerate dehydrogenase (PHGDH) further reduced the proliferation capacity of these cells (Fig. 1B), indicating that both extracellular and endogenous serine synthesis contribute to keratinocyte proliferation, with de novo serine biosynthesis unable to compensate for the lack of extracellular serine availability for proliferating keratinocytes. Under starvation conditions, primary keratinocytes also undergo terminal differentiation (Fig. 1C), not apoptosis (fig. S1A), as indicated by the decreased expression of keratin 14 (*K14*) and the increased expression of the late differentiation markers filaggrin and lorricrin (Fig. 1, C and D). To note, we confirmed that, similar to mouse keratinocytes, differentiation is triggered by the decrease in tri-methylation of lysine 27 on histone H3 (H3K27me3) and the increase in α -ketoglutarate (Fig. 1, D and E) (3). To better describe the basic metabolic phenotype of keratinocytes, we measured uptake/release rates of serine and glycine by isotope tracing (Fig. 2A). Under 0.4 mM $^{13}\text{C}_3^{15}\text{N}_1$ -serine and $^{13}\text{C}_2^{15}\text{N}_1$ -glycine supplementation, both $^{13}\text{C}_3^{15}\text{N}_1$ -serine and $^{13}\text{C}_2^{15}\text{N}_1$ -glycine levels were rapidly depleted from the medium (Fig. 2, B and C). The uptake of $^{13}\text{C}_3^{15}\text{N}_1$ -serine was 0.16 ± 0.001 μmol per million cells per hour, and the uptake of $^{13}\text{C}_2^{15}\text{N}_1$ -glycine was 0.11 ± 0.004 μmol per million cells per hour (Fig. 2B). After feeding cells with $^{13}\text{C}_3^{15}\text{N}_1$ -serine only, we detected $^{13}\text{C}_2^{15}\text{N}_1$ -glycine in the medium, indicating the intracellular conversion of serine to glycine followed by glycine efflux (Fig. 2D). When fed with $^{13}\text{C}_2^{15}\text{N}_1$ -glycine only, cells showed uptake of $^{13}\text{C}_2^{15}\text{N}_1$ -glycine and release of $^{13}\text{C}_2^{15}\text{N}_1$ -serine (Fig. 2E), indicating that $^{13}\text{C}_2^{15}\text{N}_1$ -glycine was converted to $^{13}\text{C}_2^{15}\text{N}_1$ -serine. Measurement of intracellular metabolite concentrations revealed higher $^{13}\text{C}_2^{15}\text{N}_1$ -glycine levels than $^{13}\text{C}_3^{15}\text{N}_1$ -serine in cells fed with $^{13}\text{C}_3^{15}\text{N}_1$ -serine and $^{13}\text{C}_2^{15}\text{N}_1$ -glycine (Fig. 2F). $^{13}\text{C}_2^{15}\text{N}_1$ -glycine was also detected in cells supplemented with $^{13}\text{C}_3^{15}\text{N}_1$ -serine only (Fig. 2G), which supports the notion that exogenous serine is converted to intracellular glycine. We also detected a high intracellular concentration of $^{13}\text{C}_2^{15}\text{N}_1$ -GSH in fully fed ($^{13}\text{C}_3^{15}\text{N}_1$ -serine and $^{13}\text{C}_2^{15}\text{N}_1$ -glycine) cells (Fig. 2F). When $^{13}\text{C}_2^{15}\text{N}_1$ -glycine was fed to the cells, the concentration of $^{13}\text{C}_2^{15}\text{N}_1$ -GSH increased, accompanied by the uptake of $^{13}\text{C}_2^{15}\text{N}_1$ -glycine in the cell, indicating the intracellular conversion of glycine

to GSH (Fig. 2H). When $^{13}\text{C}_3^{15}\text{N}_1$ -serine was supplemented to the cells, $^{13}\text{C}_2^{15}\text{N}_1$ -GSH was also detected at a high level (Fig. 2G), indicating that GSH was synthesized after exogenous serine converted to intracellular glycine. In cells supplemented with both stable isotope-labeled serine and glycine (Fig. 2I), $^{13}\text{C}_2^{15}\text{N}_1$ -glycine was converted to $^{13}\text{C}_2^{15}\text{N}_1$ -serine (Fig. 2J). $^{13}\text{C}_2^{15}\text{N}_1$ -glycine contributed to a small proportion of the total serine pool, which was dominated by unlabeled serine (taken up from medium and/or synthesized de novo). In cells fed with only $^{13}\text{C}_2^{15}\text{N}_1$ -glycine, $^{13}\text{C}_2^{15}\text{N}_1$ -serine was also detectable (Fig. 2K). Collectively, these results indicated that the basic metabolism of the human keratinocytes requires both exogenous serine and glycine and that the extracellular Ser/Gly availability regulates keratinocyte growth and differentiation.

SHMT2 enzyme is required for keratinocyte proliferation

Stable isotope-labeled metabolite experiments and growth curves under Ser/Gly deprivation conditions revealed that serine catabolism is crucial for keratinocytes; thus, we investigated the role of the SHMT enzymes. SHMTs metabolize serine by converting serine into glycine and THF-bound one-carbon units, linking serine catabolism to purines and thymidine synthesis. First, we investigated the expression of SHMTs at both the mRNA and protein levels and their functions (Fig. 3). Both the SHMT1 and SHMT2 enzymes were expressed in keratinocytes, with *SHMT2* mRNA five-fold more abundant than *SHMT1* (Fig. 3A). The *SHMT2* α isoform was not detected, as indicated by RNA sequencing (RNA-seq) and CAGE (cap analysis gene expression) sequencing data (Fig. 3A). Both *SHMT1* and *SHMT2* expression decreased during differentiation, as indicated by RNA-seq reads (Fig. 3A) and mRNA and protein levels in differentiated HEK1 (HEK1, normal human epidermal keratinocytes) treated with CaCl_2 for 0, 3, 6, and 9 days (Fig. 3, B and C). Confocal microscopy (fig. S1B) confirmed that mitochondrial SHMT2 was the most abundant enzyme. SHMT2 was mainly localized in the mitochondria (colocalizing with cyclophilin D) (fig. S1B), while SHMT1 was detected in the cytosol and in the nucleus (fig. S1B). We focused our attention on the mitochondrial isoform. SHMT2 was silenced by two specific small interfering RNA (siRNA) sequences (Fig. 3D), which led to a significantly reduced number of keratinocytes in the S phase, as indicated by 5-Ethynyl-2'-deoxyuridine (EdU) incorporation and cell cycle analysis (Fig. 3E and fig. S1, C and D), as well as a reduced number of clones (Fig. 3, F and G). Treatment of proliferating cells with the folate-competitive cell-permeable inhibitor of human SHMT1/2, SHIN1 (SHMT inhibitor 1) (23), at 25 μM for 48 hours strongly inhibited keratinocyte proliferation, as evaluated by EdU incorporation, cell cycle analysis, and clonogenicity assay experiments (Fig. 3, H to J, and fig. S1, E and F). SHIN1 treatment did not change SHMT2 expression levels, thereby acting as a control (Fig. 3K). These data demonstrated that the mitochondrial SHMT2 enzyme is expressed at a high level in human keratinocytes and is required to sustain keratinocyte proliferation.

SHMT2 is required for proper mitochondrial respiration

In cancer cell lines (HCT116 and Jurkat), serine catabolism by SHMT2 is required for proper mitochondrial translation initiation affecting mitochondrial oxygen consumption and cell proliferation (24, 25); therefore, we sought to determine whether SHMT2 knock-down (by siRNAs) or SHMT chemical inhibition affected

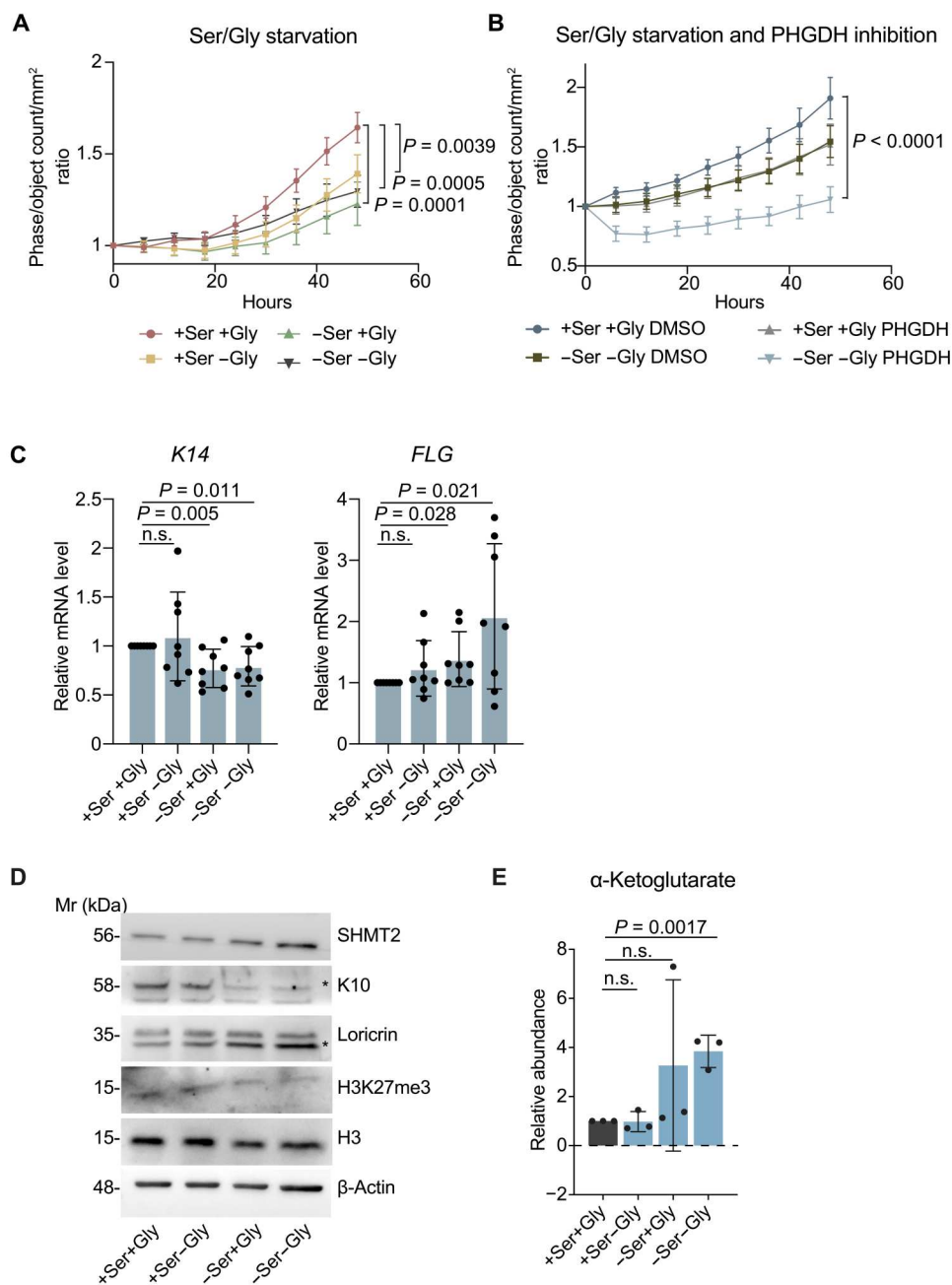


Fig. 1. Extracellular serine and glycine are required for keratinocyte proliferation. (A) Growth curve by confluence ratio of human keratinocytes (Kert-CT) after serine/glycine (Ser/Gly) starvation ($n = 4$). (B) Growth curve by confluence ratio of Kert-CT cells after Ser/Gly starvation and PHGDH inhibition ($1 \mu\text{M}$) ($n = 3$). For statistical analysis, one-way analysis of variance (ANOVA) test was performed. (C) Real-time quantitative polymerase chain reaction (RT-qPCR) of *K14* and *Filaggrin* mRNAs after Ser/Gly starvation ($n = 8$). (D) Western blot for H3K27me3 and differentiation markers (loricrin and K10) in Gly/Ser deprivation. H3 and β -actin are shown as control (one representative experiment of $n = 3$ is shown). Mr, Mass relative. (E) Representative intracellular α -ketoglutarate level ($n = 3$ biologically independent samples). P values are calculated, comparing starving cells to cells grown in normal medium. n.s., not significant.

mitochondrial functions and/or cellular respiration in primary proliferating human keratinocytes. Using MitoSOX Red staining, we found a modest increase in the mitochondrial superoxide anion content upon SHMT2 silencing (Fig. 4, A and B). We did not observe substantial changes in mitochondrial membrane potential, mitochondrial DNA (mtDNA) content (*mtND1*), translation rate of mitochondrial protein Cytochrome c oxidase subunit 4 (COX-IV),

or defects in the expression of electron transport chain (ETC) complexes (Fig. 4, C to F). The mitochondrially encoded protein Cytochrome c oxidase I (MTCO1) was expressed at normal level, confirming that SHMT2 silencing, allowing the expression of SHMT2 at a low level (Fig. 3A), does not affect the translation of mitochondrial proteins (25). To further analyze the impact of SHMT2 in shaping central metabolism, we assessed the energetic

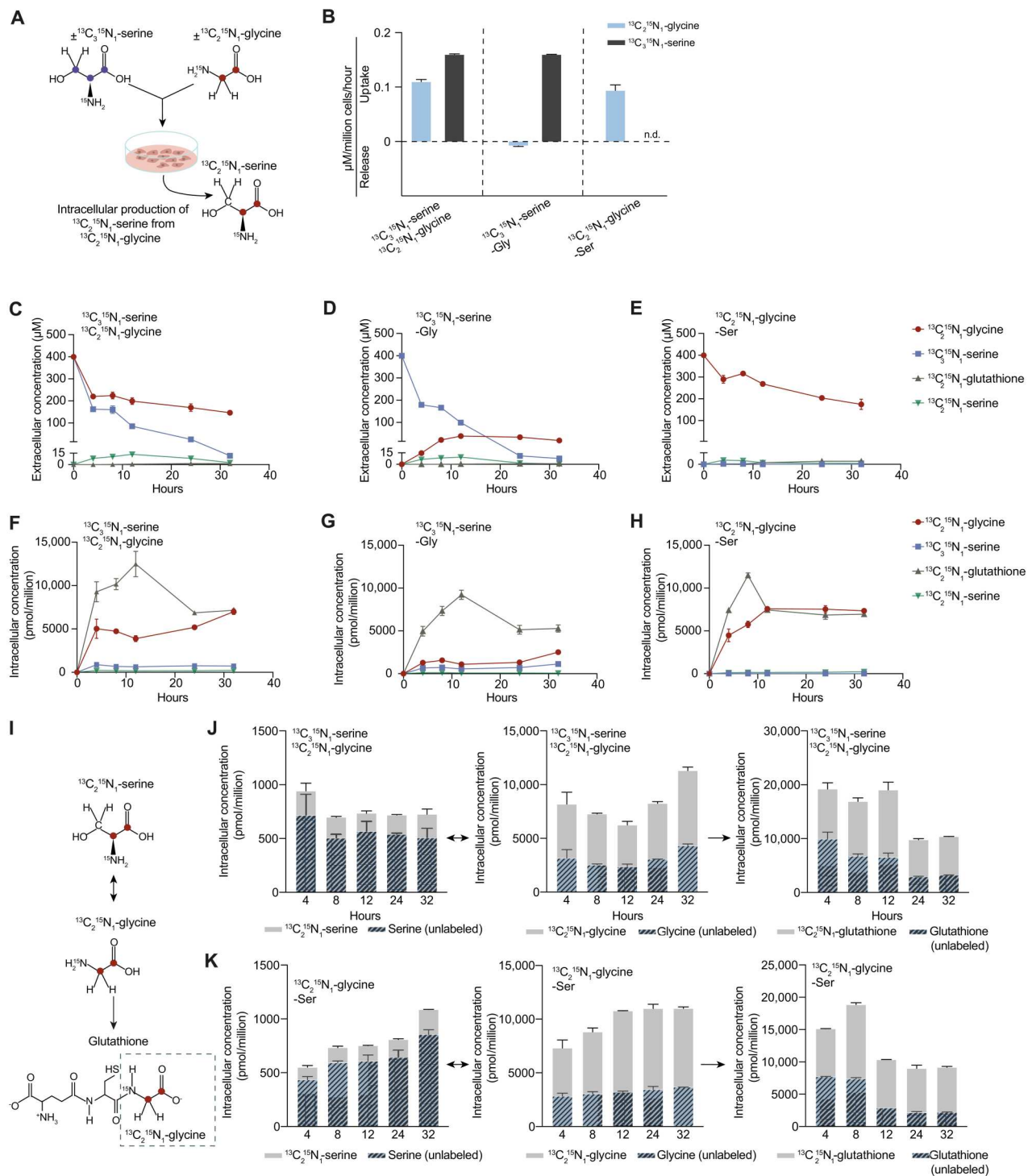


Fig. 2. Basic metabolism of keratinocyte required exogenous serine and glycine. (A) Scheme of stable isotope-labeling experiments. (B) $^{13}\text{C}_3^{15}\text{N}_1$ -serine and $^{13}\text{C}_2^{15}\text{N}_1$ -glycine uptake and release over 32 hours using ultra-performance liquid chromatography–quadrupole time-of-flight mass spectrometry (UPLC-QTOF-MS) normalized to cell number grown in the indicated media. Data are means of duplicate wells; bars represent SD. n.d., not determined. (C to E) Extracellular concentration of labeled metabolites in keratinocyte grown in the indicated combination of media containing 0.4 mM labeled ($^{13}\text{C}_3^{15}\text{N}_1$)-serine and/or 0.4 mM labeled ($^{13}\text{C}_2^{15}\text{N}_1$)-glycine. Media were sampled at indicated time points and analyzed by UPLC-QTOF-MS. Data are means of duplicate wells; bars represent SD. (F to H) Intracellular concentration of labeled metabolites, in keratinocyte grown in the indicated combination of media containing 0.4 mM labeled ($^{13}\text{C}_3^{15}\text{N}_1$)-serine and/or 0.4 mM labeled ($^{13}\text{C}_2^{15}\text{N}_1$)-glycine. Media were sampled at indicated time points and analyzed by UPLC-QTOF-MS. Data are means of duplicate wells; bars represent SD. (I) Scheme of labeled Gly and Ser conversion and derived GSH. (J and K) Metabolic fluxes indicating intracellular metabolites (Ser, Gly, and GSH) extracted and analyzed via UPLC-QTOF-MS. Keratinocytes were grown in the indicated combination of media containing 0.4 mM labeled ($^{13}\text{C}_3^{15}\text{N}_1$)-serine and/or 0.4 mM labeled ($^{13}\text{C}_2^{15}\text{N}_1$)-glycine. Data are means of duplicate wells; bars represent SD.

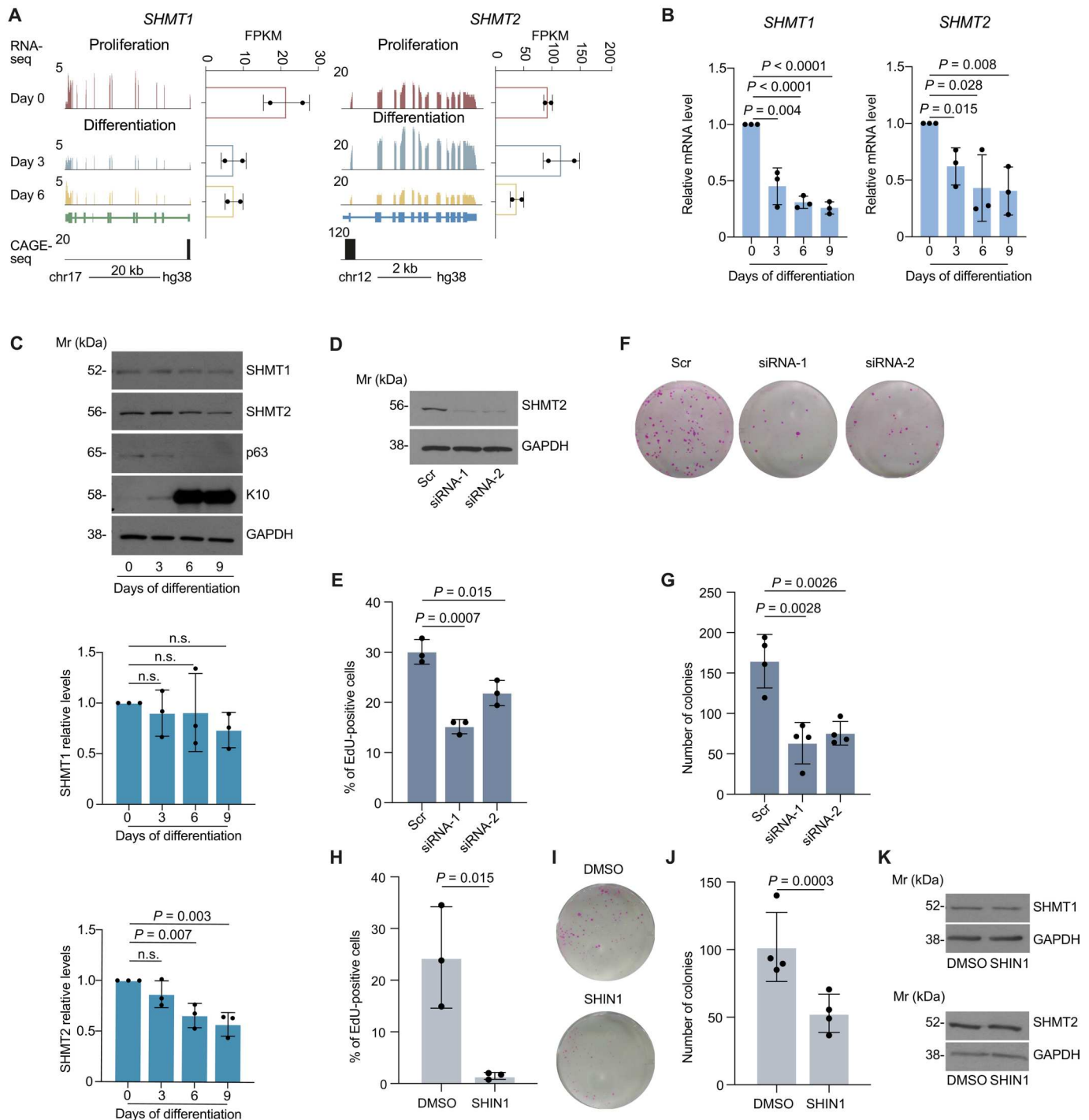


Fig. 3. SHMT2 enzyme is required for keratinocyte proliferation. (A) SHMT expression indicated by RNA-seq in proliferating (ENCSR527SSD) and differentiating (ENCSR959LTT and ENCSR034RPU) keratinocytes, ENCODE database (www.encodeproject.org/). CAGE sequencing (CAGE-seq) for *SHMT1* and *SHMT2* available on ENCODE (GSM849367). FPKM, fragments per kilobase of exon per million mapped. (B) RT-qPCR of *SHMT1* and *SHMT2* mRNAs in in vitro differentiated keratinocytes (0, 3, 6, and 9 days of differentiation by calcium chloride) and relative ratio of *SHMT1* and *SHMT2* expression normalized to glyceraldehyde-3-phosphate dehydrogenase (GAPDH). p63 and K10 were shown as proliferation and differentiation controls. One representative experiment is shown ($n = 3$). (C) Western blot of SHMT in in vitro differentiated keratinocyte (0, 3, 6, and 9 days of differentiation by calcium chloride) and relative ratio of SHMT1 and SHMT2 expression normalized to glyceraldehyde-3-phosphate dehydrogenase (GAPDH). p63 and K10 were shown as proliferation and differentiation controls. One representative experiment is shown ($n = 3$). (D) Western blot (one representative experiment of three is shown) confirms SHMT2 silencing. (E) EdU-positive keratinocytes after 72 hours of SHMT2 silencing ($n = 3$). (F) Keratinocyte clonogenicity assay after 48 hours of SHMT2 silencing. (G) Quantification of colonies in control (Scr) and SHMT2-silenced samples (siRNA-1 and siRNA-2) ($n = 4$). (H) EdU-positive keratinocytes after 48 hours of treatment with dimethyl sulfoxide (DMSO) and SHIN1 ($n = 3$). (I) Clonogenicity assay of DMSO or SHIN1 (25 μ M) after 48 hours of treatment. (J) Quantification of colonies in control (DMSO) and treated (SHIN1) cells ($n = 4$). (K) Western blots (one representative experiment of three is shown) showing SHMT expression after SHIN1 treatment. For all the experiments, a P value was obtained using Student's t test. Values were considered significant when $P < 0.05$.

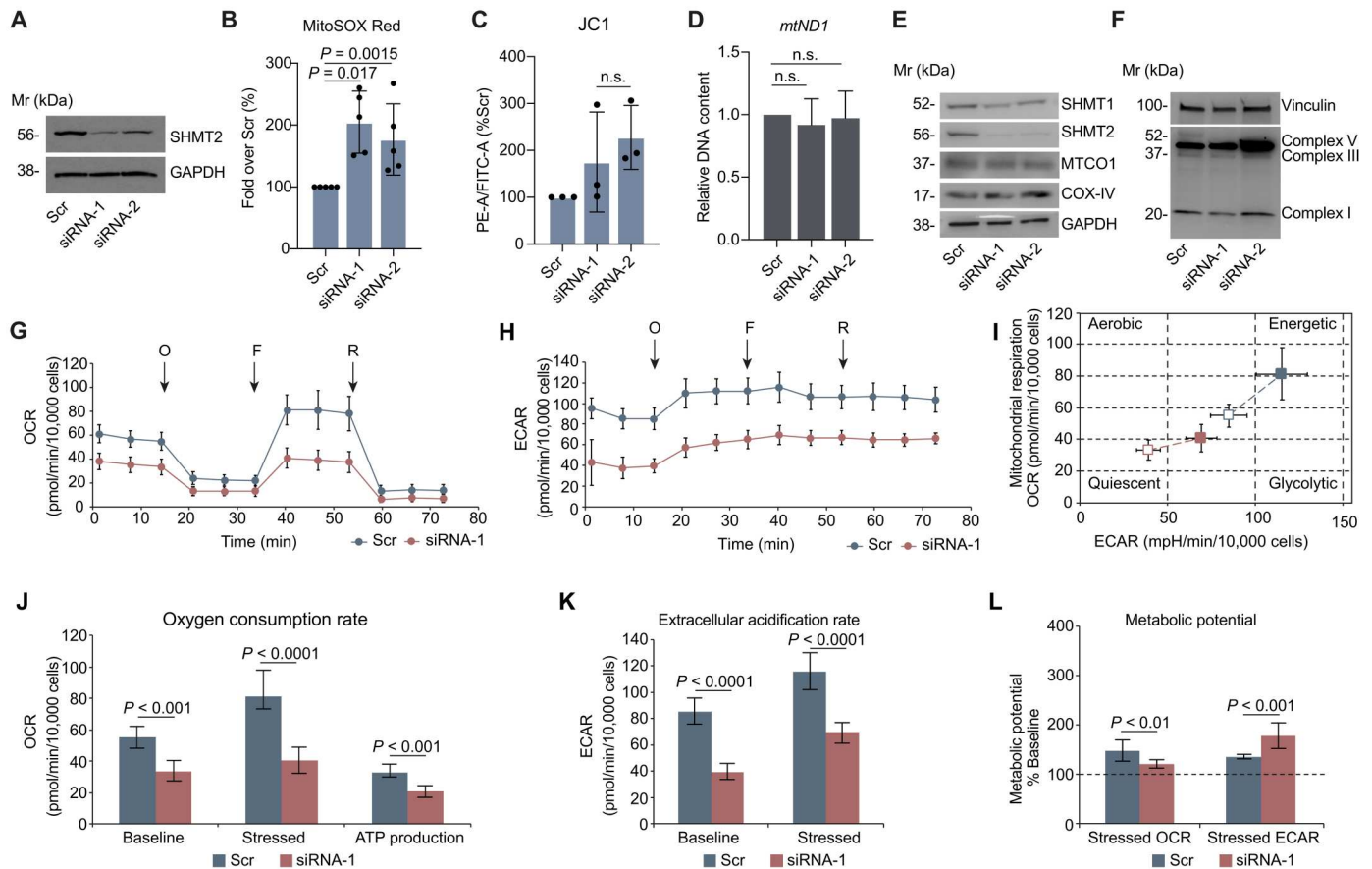


Fig. 4. SHMT2 enzyme is required for proper mitochondrial respiration and function. (A) Western blot confirmed SHMT2 silencing. (B) MitoSOX Red staining after SHMT2 silencing; red fluorescence [phycoerythrin–Area (PE-A)] was measured ($n = 5$). (C) JC1 staining after SHMT2 silencing. The red fluorescence (PE-A) and green fluorescence [fluorescein isothiocyanate–Area (FITC-A)] were measured ($n = 3$). (D) mtDNA content in HEK293T cells after SHMT2 silencing ($n = 3$). (E) Western blot of MTCO1 encoded by mitochondrial genome and translated in mitochondria and of COX-IV encoded by nuclear genome and translated in the cytoplasm after SHMT2 silencing. (F) Western blot of mitochondrial ETC proteins after SHMT2 silencing. (G) Keratinocyte mitochondrial respiration obtained by means of OCR and compared to control (Scr) after SHMT2 silencing. Arrows indicate the addition of drugs used to target a specific mitochondrial function. O, oligomycin; R, rotenone + antimycin. (H) Glycolysis rate after SHMT2 silencing determined with the ECAR. (J and K) Average values of (G) and (H). (I) Phenotype plot as variation of both basal ECAR and OCR under stress conditions (upon addition of the drugs). (L) Metabolic potential as a percentage of the stress conditions over the basal conditions. For all the Western blots, one representative experiment of three is shown. For the Seahorse assay, a representative experiment is shown. Values are the means of at least 8 replicates \pm SD. P values were obtained by Student's t test for all the experiments except for the Seahorse analysis, in which the one-way ANOVA followed by Bonferroni post hoc comparison was used; $P < 0.05$ and $P < 0.01$ are considered statistically significant.

profile of keratinocytes with a Cell Mito Stress Test kit using a Seahorse extracellular flux analyzer. As reported in Fig. 4 (G and J), siRNA-targeting SHMT2 caused a reduction in both basal respiration and maximal respiratory capacity; this negative effect also led to significantly reduced adenosine triphosphate production (Fig. 4J). The reduced mitochondrial activity was not balanced by basal glycolysis, which was also lowered in the silenced samples (Fig. 4, H and K). In general, the energetic phenotype of the silenced samples was replaced with a quiescent phenotype, compared to the control, and the effect was appreciable on both respiration and glycolysis (Fig. 4, I and L). Nevertheless, under stress conditions [i.e., in the presence of oxidative phosphorylation (OXPHOS)-targeting drugs], the maximal glycolytic potential in the silenced sample was higher than that in the untreated sample (Fig. 4L), suggesting that metabolic quiescence is finely tuned and that glycolytic pathways alone could be promptly activated when necessary. When

challenged with carbonyl cyanide *p*-trifluoromethoxyphenylhydrazone (FCCP), SHMT2-silenced cells exhibited an increase in oxygen consumption rate (OCR) (Fig. 4, G and J), indicating a functional ETC. Considering these findings, we also investigated the effect of SHIN1 treatment on the cellular energy profile (Fig. 5, A to L). SHIN1-treated cells, instead, showed a reduction of the mitochondrially encoded protein MTCO1 (Fig. 5E). SHIN1 treatment had a marked effect on both the OCR (Fig. 5, G and J) and the extracellular acidification rate (ECAR) (Fig. 5, H and K), and, globally, the phenotype was markedly more quiescent than that of the untreated sample (Fig. 5, I to L). The discrepancy between mitochondrially encoded protein MTCO1 expression is due to the level of SHMT2 depletion (Fig. 4E) or inactivation (Fig. 5E), being SHIN1 very effective to inhibit SHMT2 activity as demonstrated by metabolomics (see Fig. 6, B and C). Low levels of SHMT2 protein/activity, which is the case when using siRNA silencing (see Fig. 4A),

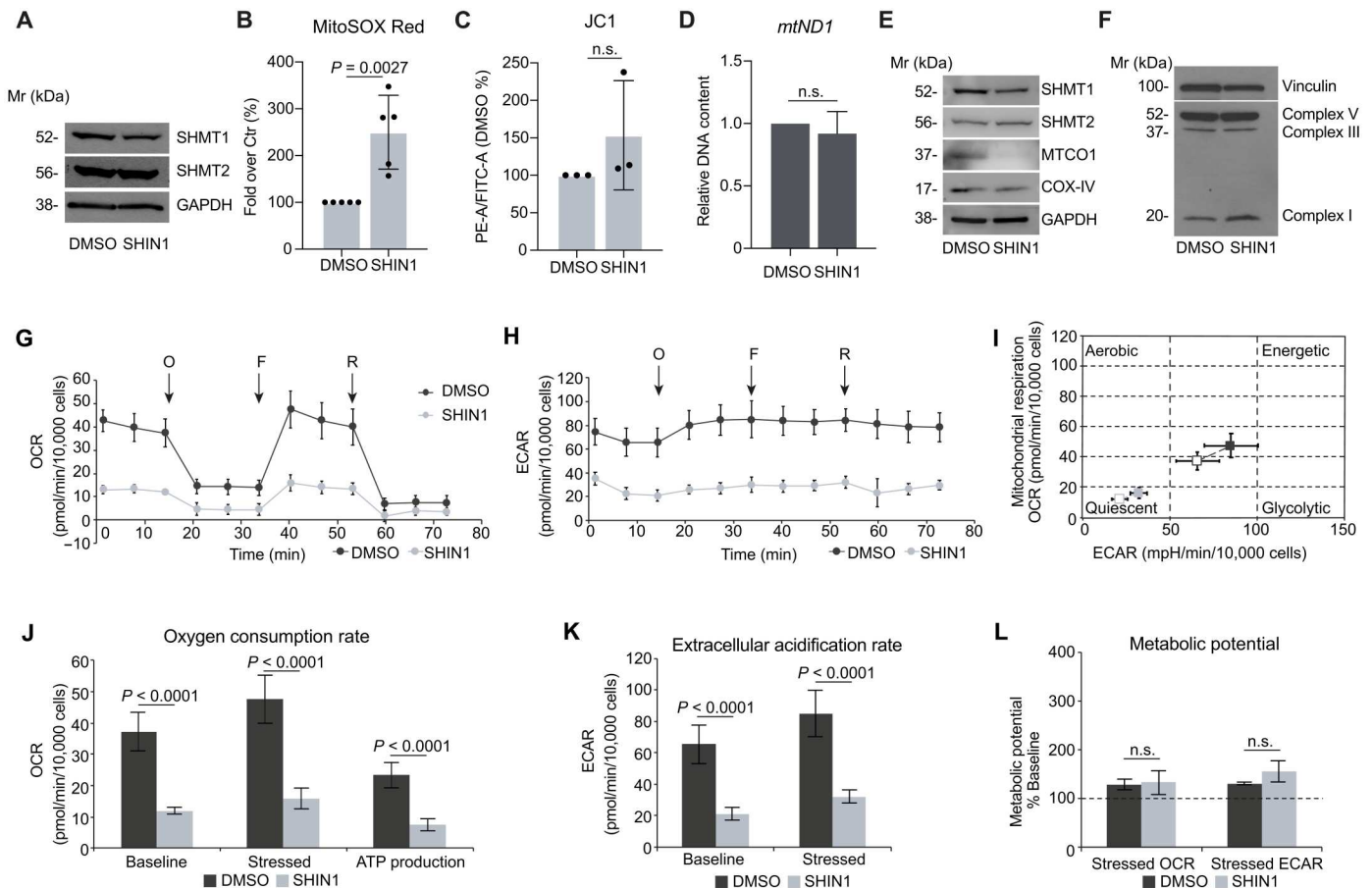


Fig. 5. SHMT inhibition affects mitochondrial function and mitochondrial translation. (A) Western blot of SHMT enzyme expression after DMSO or SHIN1 treatment. (B) MitoSOX Red staining was performed after SHMT inhibition with SHIN1 (25 μ M); red fluorescence (PE-A) was measured ($n = 5$). (C) JC1 staining after SHMT inhibition with SHIN1 (25 μ M); the red fluorescence (PE-A) and green fluorescence (FITC-A) were measured ($n = 3$). (D) mtDNA content after SHMT inhibition with SHIN1 (25 μ M) ($n = 3$). (E) Western blot for MTCO1 and COX-IV after SHMT inhibition with SHIN1 (25 μ M). (F) Western blot for mitochondrial ETC proteins after SHIN1 treatment. (G) Mitochondrial respiration after SHIN1 treatment as determined by OCR measured through seahorse experiments. (H) Glycolysis rate determined with the ECAR. (J and K) Average values of the indicated parameters. (I) Phenotype plot as the variation in both basal ECAR and OCR under stress conditions (upon addition of the drugs). (L) Metabolic potential as a percentage of the stress conditions over the basal ones. For all the Western blots, one representative experiment of three is shown. For the seahorse assay, a representative experiment is shown, and the values reported in the plot are the means of 8 replicates \pm SD. P values were obtained by Student's t test for all the experiments except for the seahorse analysis, in which the one-way ANOVA followed by Bonferroni post hoc comparison was used; $P < 0.05$ and $P < 0.01$ are considered statistically significant.

are sufficient to restore translation of mitochondrial proteins (25). These results indicate that the reduced OCR in siSHMT2 keratinocytes is a consequence of decreased proliferation rate and thus decreased metabolic demands (Fig. 3, F and G, and fig. S1, C and D), while in SHIN1-treated cells, a combination of decreased proliferation rate (Fig. 3, H to J, and fig. S1, E and F) and defective mitochondrial translation contributes to the marked drop of the mitochondrial functions.

SHMT2 deficiency alters keratinocyte central metabolism and induces purines and GSH depletion

To define the impact of SHMT2 knockdown and SHMT inhibition on central metabolism and which specific aspect of serine metabolism is the most relevant to the decreased keratinocyte proliferation, we performed a metabolomic profile. Six biological replicates of control [scramble-treated (Scr)], SHMT2-silenced (siRNA-1), and SHIN1-treated keratinocytes were analyzed (Fig. 6, A to J, and

figs. S2 to S4). First, we confirmed that SHMT2 knockdown or inhibition resulted in a significant decrease in glycine levels (Fig. 6, B and C), confirming that the SHMT2 enzyme is primarily responsible for intracellular glycine synthesis (Fig. 2, C to K). The activation of the de novo serine biosynthetic pathway was probably delayed, as indicated by the accumulation of glycerate 3-phosphate (3-P) and glyceraldehyde-3P, while 3-phospho-serine levels did not significantly change (figs. S2A and S3A). The glycolytic endpoint products pyruvate and lactate and tricarboxylic acid cycle products were not significantly affected in the control or SHMT2-silenced cells (fig. S2C), suggesting that these metabolites are moderately altered under the experimental conditions used. In line with proliferation reduction (Fig. 3, A and B), SHMT2 silencing or inhibition led to a decrease in the pentose phosphate pathway intermediates erythrose-4P and ribose-5P, which are necessary for nucleic acid and nucleotide biosynthesis (figs. S2B and S3B). Pyruvate and lactate levels (figs. S2C and S3C) decreased, indicating a limited

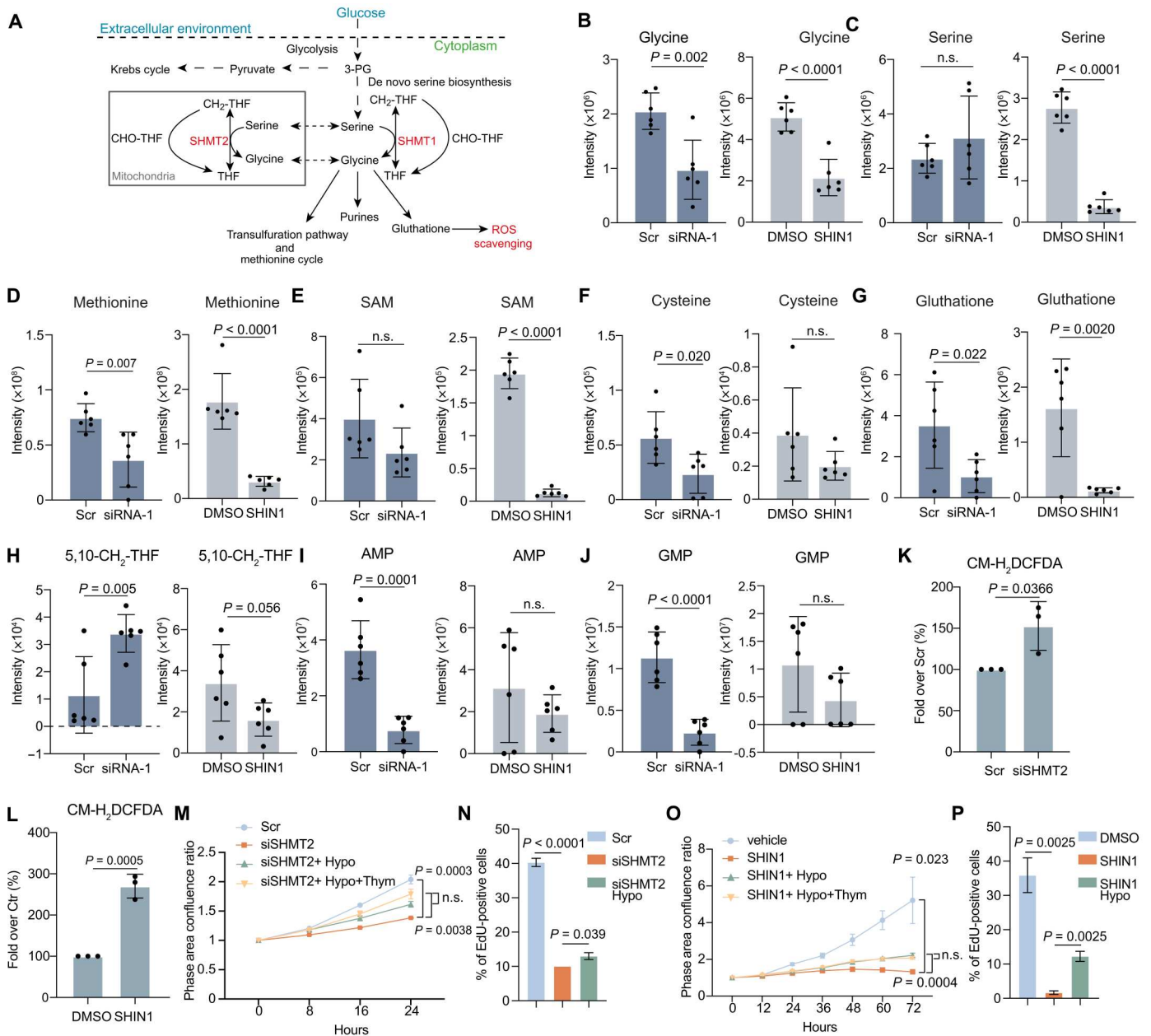


Fig. 6. SHMT2 controls central metabolism and contributes to purine and GSH synthesis. (A) Schematic representation of intracellular serine and glycine metabolism and one-carbon units used in cytoplasm and mitochondria pathways. PG, 3-phosphoglycerate; CHO-THF, Formyltetrahydrofolate. (B to J) Metabolomic analysis of glycine (B), serine (C), methionine (D), S-adenosylmethionine (SAM) (E), cysteine (F), GSH (G), 5,10-CH₂-THF (H), adenosine monophosphate (AMP) (I), and guanosine monophosphate (GMP) (J) in keratinocytes after SHMT2 silencing or SHIN1 treatment. (K) Total ROS staining with CM-H₂DCFDA in Ker-CT after SHMT2 silencing; green fluorescence (FITC-A) was measured by flow cytometry (n = 3). (L) Total ROS staining with CM-H₂DCFDA in Ker-CT cells after SHIN1 treatment; green fluorescence (FITC-A) was measured by flow cytometry (n = 3). (M) Growth curve by confluence ratio of Kert-CT after SHMT2 silencing and hypoxanthine without thymidine supplementation (n = 3). (N) EdU-positive cells after SHMT2 silencing and hypoxanthine supplementation (n = 3). (O) Growth curve by confluence ratio after SHIN1 treatment and hypoxanthine without thymidine supplementation (n = 3). (P) EdU-positive cells after SHMT2 silencing and hypoxanthine supplementation (n = 3). For growth curves statistical analysis, one-way ANOVA was performed. For metabolic analysis and EdU experiments, P values were obtained using Student's t test. P < 0.05 was considered significant.

Downloaded from https://www.science.org on January 29, 2023

capacity of keratinocytes to compensate for reduced glycolysis, confirming the cellular respiration data (Figs. 4, H and K, and 5, H and K).

SHMT2 silencing or inactivation also affected the methionine cycle and trans-sulfuration pathway, as indicated by the reduction in methionine, *S*-adenosylmethionine, and cysteine (Fig. 6, D to F). The strong reduction of glycine also resulted in a marked decrease in GSH (Figs. 2, C to K, and 6G). One-carbon units formed upon serine deprivation are also used for *de novo* synthesis of adenosine, guanosine, and thymidylate. Among the detectable metabolites, we found that nucleotide adenosine monophosphate (AMP) and guanine monophosphate had the tendency to or were significantly reduced in SHMT2-silenced or SHIN1-treated keratinocytes, respectively (Fig. 6, I and J). 5,10-Methylenetetrahydrofolate (5,10-CH₂-THF) was significantly reduced in SHIN1-treated keratinocytes (Fig. 6H). In siSHMT2 cells, instead, 5,10-CH₂-THF increased possibly as a compensatory mechanism from the cytosolic one-carbon THF intermediates. Together, these results indicate that SHMT2 inhibition or reduction causes purines depletion. Metabolomics indicated that depleted purines and GSH are the relevant affected metabolites. To further investigate these findings, we performed rescue experiments using small molecules. As expected, reactive oxygen species (ROS) levels increased in SHMT2 silencing or SHIN1 treatment (Fig. 6, K and L), and the addition of GSH in the culture medium did not rescue cell proliferation (fig. S4, A and B). Hypoxanthine supplementation, but no thymine, partially rescued growth in SHMT2-silenced or SHMT2-inhibited keratinocytes (Fig. 6, M to P). Thymidine, which rescues the effects of the classic antifolate but does not contain glycine, had no benefit in SHIN1-treated or SHMT2-silenced keratinocytes. Supplementation with only formate did not rescue keratinocyte proliferation (fig. S4, C and D). Last, to check whether keratinocytes could compensate mitochondrial formate loss by reversal of cytosolic one-carbon metabolism, we silenced Methylenetetrahydrofolate Dehydrogenase (NADP⁺ Dependent) 1 Like (MTHFD1L). Metabolite array showed that siMTHFD1L has no impact on keratinocytes metabolism, confirming that one-carbon metabolites generated in the cytosol are provided to the mitochondria (fig. S4E and table S1). In addition, double siSHMT2-siMTHFD1L restored keratinocyte proliferation due to SHMT2 silencing (fig. S4, F and G) thanks to the glycine compensation (fig. S4E and table S1). The compensation is abrogated using SHIN1 inhibitor (fig. S4, H and I). SHIN1 blocking both SHMT1/2 isoforms abrogated the hydroxymethyl group cleaved from serine that can enter the THF cycle, providing a significant reduction of one-carbon units for methylation reactions. Overall, the experiments demonstrated that SHMT2 silencing/inactivation strongly affected serine and glycine metabolism. Hypoxanthine supplementation recovered keratinocyte proliferation, confirming that purines synthesis is the more relevant SHMT2-dependent metabolic pathway needed to sustain keratinocyte proliferation.

SHMT inhibition ameliorates the psoriasiform phenotype in an imiquimod-induced mouse model of psoriasis

The data obtained thus far clearly demonstrated through SHMT chemical inhibition and/or SHMT2 knockdown that these enzymes are crucial for energetic metabolism and the provision of precursors to support keratinocyte growth. We next determined whether SHMTs are involved in skin hyperproliferative diseases,

such as psoriasis, a chronic inflammatory disease characterized by inflammation, keratinocyte hyperplasia, and abnormal differentiation (26–28). Using the imiquimod (IMQ)-induced psoriasiform mouse model and inducing both epidermal hyperplasia and inflammatory cell infiltration into the dermis and epidermis (29, 30), we tested the effect of topical SHIN1 treatment administered with 1 mM IMQ for 5 days (treated as shown in Fig. 7A). Topical inhibition of SHMT enzymatic activity substantially reversed the psoriasis-like phenotype in the IMQ-treated mice (Fig. 7, B to H, and fig. S5, A and B) and reduced psoriasiform signs, including epidermal and scale thickness, as assessed by quantifying the average of these parameters based on images of hematoxylin and eosin (H&E)-stained skin sections (Fig. 7, B and C). SHIN1 treatment also attenuated widespread inflammatory cell infiltration in the dermis compared with that in IMQ-treated mice (Fig. 7, B and C). The skin of IMQ + SHIN1-treated mice showed significantly reduced Ki67 staining compared to vehicle-treated controls (IMQ and SHIN1; Fig. 7, D and E) and restored compartmentalization and expression of differentiation markers, such as K10 (Fig. 7D). K10 immunostaining was rather weak in the suprabasal layer of the epidermis in the IMQ-treated mice, whereas it was comparable to that in the control mice when IMQ was coadministered with SHIN1 (Fig. 7D). In addition to defects in proliferation/differentiation processes, IMQ treatment induced dermal accumulation of inflammatory cells, including neutrophils, macrophages, and T cells (29, 31). In the skin, IMQ also markedly induced the expression of chemokines with effects on interleukin-17A (IL-17A)- and IL-22-producing cells, two leukocyte subpopulations pathogenically active in the IMQ model.

Hence, we examined the effects of SHIN1 on IMQ-induced skin inflammation by immunohistochemistry and real-time quantitative polymerase chain reaction (RT-qPCR). We found a significantly decreased number of neutrophils (LY6G⁺ cells) in the skin of IMQ + SHIN1-treated mice (Fig. 7, D and F) compared to IMQ-treated mice and a similar quantity of CD3⁺ cells (Fig. 7, D and G). In addition, we observed a significant reduction in *Ccl20* (Fig. 7H) and *CxCl16* (Fig. 7H), which affect IL-17A-producing $\gamma\delta$ T cells that are usually expanded and activated under acute and chronic skin inflammatory conditions, such as psoriasis, suggesting that SHIN1 treatment potentially reduced the number of $\gamma\delta$ T cells or inhibited their activation. Consistently, RT-qPCR analysis showed that the mRNA expression of the cytokines *Il-22* and *Il-17a* was significantly decreased in the skin of IMQ + SHIN1-treated mice compared to IMQ-treated mice (Fig. 7H). The expression of other cytokines/chemokines and psoriasis-related molecules (i.e., *Tnf-a*, *Il-1b*, *Il-36 g*, *CxCl1*, *CxCl10*, and *S100a7*) was only slightly decreased in IMQ + SHIN1-treated skin compared to IMQ-treated skin; the difference was not statistically significant (fig. S5A). We showed that SHIN1 treatment did not affect SHMT2 expression, serving as a control (fig. S5B). Together, these results show that SHMT inhibition in the IMQ-psoriasiform mouse model restores epidermal homeostasis, prevents inflammatory cell recruitment, and reduces pathological cytokines production.

SHMT2 is expressed at high levels in human psoriatic skin lesions

To extend the translational relevance of these findings, we evaluated the expression of *SHMT1* and *SHMT2* in the GSE13355 public dataset containing mRNA expression data obtained from healthy

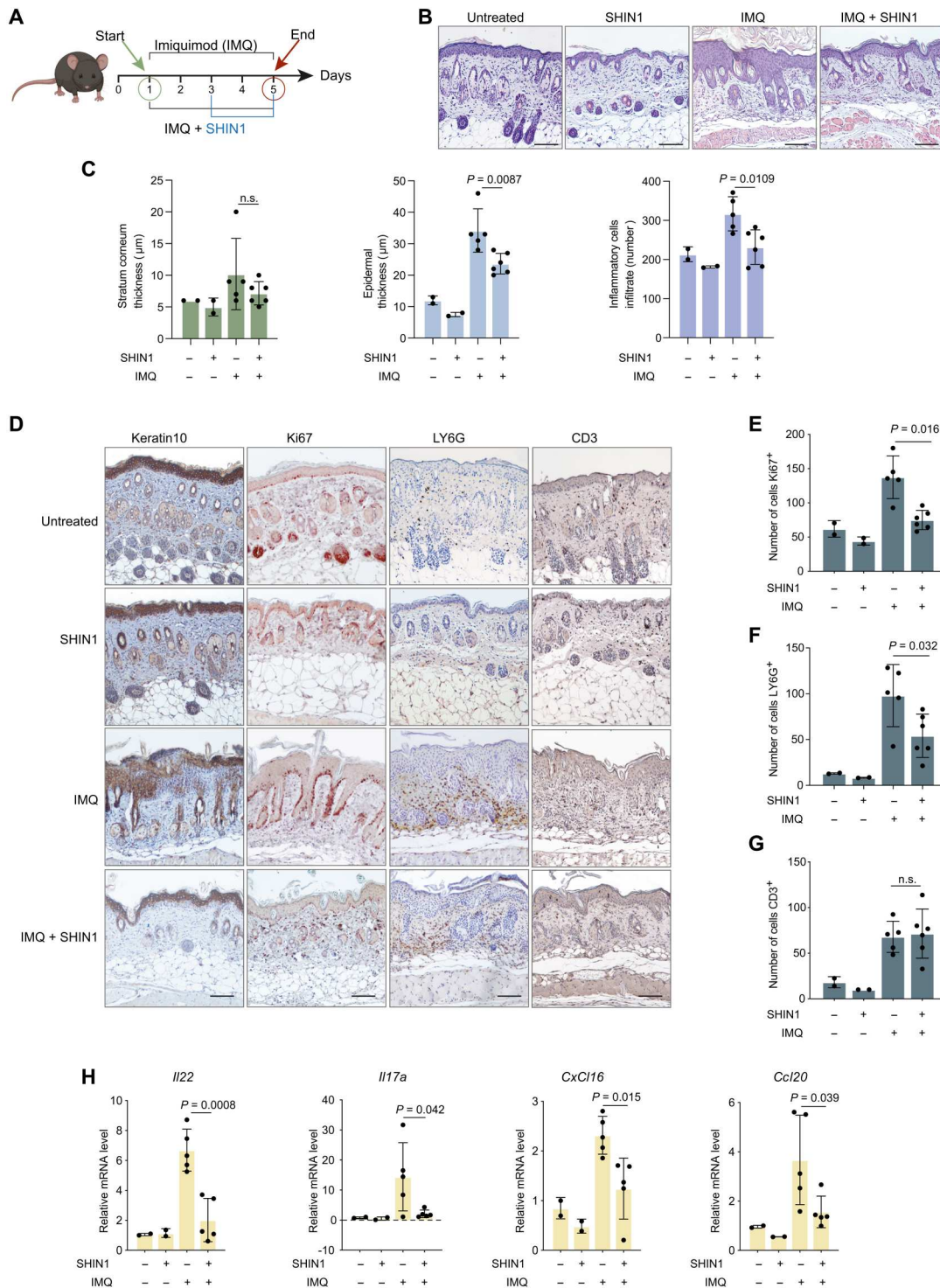


Fig. 7. Chemical inhibition of SHMTs decreases IMQ-induced psoriasisform hyperplasia and skin inflammation. (A) Scheme of the experiment performed on mouse skin to induce psoriasis-like lesions with IMQ, partially generated using Biorender.com. (B) H&E staining of untreated skin ($n = 2$), SHIN1-treated skin ($n = 2$), skin treated with IMQ ($n = 6$), and skin treated with IMQ and SHIN1 ($n = 6$). Scale bars, 200 μm. (C) Measurement of stratum corneum thickness, epidermal thickness, and the number of inflammatory cells infiltrating the dermis. (D) Immunohistochemistry staining for K10, Ki67, Ly6G, and Cd3 and (E) the corresponding quantification of proliferation (Ki67) and inflammatory cell markers (F and G). Scale bars, 200 μm. (H) Gene expression analysis of some inflammatory markers in untreated mouse skin ($n = 2$), treated with SHIN1 ($n = 2$), treated with IMQ ($n = 5$), and treated with the combination of IMQ and SHIN1 ($n = 5$) as determined by RT-qPCR. For all the experiments, a P value was obtained using Student's t test. $P < 0.05$ was considered significant.

skin ($n = 64$), nonlesional psoriatic skin ($n = 54$), and lesional psoriatic skin ($n = 54$). The bioinformatics analysis showed a significant increase in *SHMT2* mRNA levels in the psoriatic lesional epidermis compared with the nonlesional and normal epidermis (Fig. 8A), suggesting that serine catabolism is required for psoriatic pathology. Changes were not detected in *SHMT1*, indicating different roles of these isoforms in psoriasis pathology (Fig. 8A). These results were confirmed with skin biopsy samples obtained from psoriatic patients ($n = 6$ lesional psoriatic skin samples and $n = 6$ nonlesional psoriasis skin samples) compared to normal healthy controls. RT-qPCR analysis confirmed that only *SHMT2* mRNA was overexpressed in psoriatic skin biopsy samples, reaching statistical significance for both nonlesional and lesional samples ($P = 0.0118$ and $P = 0.0015$, respectively) (Fig. 8B). The results were also confirmed at the protein level (Fig. 8C).

We checked *SHMT1/2* expression of in other inflammatory skin disorder datasets, including atopic dermatitis (fig. S6, A and B), and in neoplastic skin diseases (basal cell carcinomas and squamous cell carcinomas; fig. S6C). *SHMT1/2* expression does not significantly change in the datasets analyzed, suggesting that *SHMT2* overexpression is specifically linked to psoriasis. The serine de novo biosynthetic enzymes *PHGDH*, *PSAT1*, and *PSPH* were also up-regulated in the GSE13355 public Gene Expression Omnibus (GEO) dataset (fig. S6D), indicating a role for both extracellular and endogenous serine in psoriasis. To determine the link between one-carbon units derived from serine and the THF cycle, we analyzed the expression levels of cytosolic THF cycle enzymes (*DHFR*, *MTHFR*, and *MTHFD1*) and mitochondrial THF cycle enzymes (*MTHFD1L*, *MTHFD2*, and *MTHFD2L*) and found that most of these enzymes were significantly up-regulated in lesional and nonlesional psoriatic skin (fig. S6E), suggesting a key role for these enzymes in psoriasis pathogenesis. Together, the data presented clearly indicate that in vitro and in vivo serine catabolism and one-carbon metabolism have an important role in skin diseases involving keratinocyte hyperplasia, abnormal differentiation, and inflammation.

DISCUSSION

The epidermis protects organisms against water loss and environmental stress. It is also a self-renewing tissue with somatic stem cells that divide to sustain progenitor basal cells through differentiation. How nutrients availability contributes to these processes in normal and pathological diseases had not been investigated. In this study, we demonstrated that extracellular serine and the mitochondrial *SHMT2* enzyme play an important role in controlling human keratinocyte proliferation and differentiation (Figs. 1 and 3). Ser/Gly deprivation experiments showed that human keratinocytes rely on exogenous serine and glycine to proliferate. This aspect differs from mouse epithelial stem cells in which serine auxotrophy appears only under premalignant or malignant (3) conditions. In proliferating cells, even in the presence of other parallel cytoplasmic pathways, *SHMT2* uses extracellular serine to generate glycine and a folate one-carbon unit, which produces THF-conjugated one-carbon units used in cytoplasmic reactions (Fig. 2, C to K), indicating the relevance of serine catabolism and *SHMT2* in epithelial biology (Fig. 8D). *SHMT2* depletion or its chemical inactivation resulted in a decrease in oxygen consumption and the unbalanced energetic demand through glycolytic pathways (Figs. 4 and 5). Metabolomics

and stable isotope labeling (Figs. 2 and 6 and figs. S2 to S4) confirmed that *SHMT2* was primarily responsible for glycine formation and for purines biosynthesis [AMP and guanosine monophosphate (GMP)], GSH, trans-sulfuration, and methionine pathways that were significantly reduced. Rescue experiments with hypoxanthine (\pm thymidylate), GSH, and formate indicated that only hypoxanthine supplementation partially rescued growth in keratinocytes (Fig. 6, M to P). Thymidine, which rescues the effects of the classic antifolate but does not contain glycine, had no benefit in SHIN1-treated or *SHMT2*-silenced keratinocytes. Thus, *SHMT2* silencing and SHIN1 treatments block cell growth through a progressive depletion of purines, leading to loss of nucleotide triphosphates. Proliferating keratinocytes also consume glycine at baseline (Fig. 2). This metabolic peculiarity could be due to the keratinocytes that need to maintain a high level of antioxidant defense (GSH) against external stressors (i.e., ultraviolet radiation).

Because serine/glycine availability and *SHMT2* enzymes are required for human keratinocyte proliferation, we thought that *SHMT2* depletion/inhibition might represent a promising therapeutic approach for psoriasis, a chronic skin disease characterized by excessive, cytokine-driven epidermal hyperplasia (32). Psoriasis is an immune-mediated, genetic disease, with an estimated prevalence of 3% in the worldwide population (32–34).

Using the IMQ-induced psoriasiform mouse model, topical application of the *SHMT* inhibitor SHIN1 was effective in protecting mice from presenting with IMQ-induced psoriasiform signs, including an increase in epidermal hyperplasia (Fig. 7), as shown by a decrease in epidermal and scale thickness and a reduction in Ki67-positive cells. This result paralleled the effect of *SHMT2* depletion/inhibition on the proliferation of normal human keratinocytes (Fig. 3). Consistent with the previously reported roles of *SHMTs* and serine metabolism in T cell expansion and activation (19), SHIN1 treatment was effective in protecting the mouse from IMQ-induced inflammation, as shown by the decrease in infiltrating inflammatory cells (neutrophils in particular) and the decrease in the expression of psoriasis cytokines and chemokines associated with $\gamma\delta$ T cell recruitment and activation (Fig. 7 and fig. S5). We demonstrated that the expression of the *SHMT2* enzyme, but not *SHMT1*, was elevated at the mRNA and protein levels in patients' lesional and nonlesional psoriatic plaques (Fig. 8, B and C). A meta-analysis of available datasets (Fig. 8 and fig. S6) confirmed *SHMT2* overexpression in psoriatic skin lesions, while no overexpression for *SHMT1* and *SHMT2* was observed for atopic dermatitis and basal cell carcinomas (fig. S6, A to C). Note that many cytosolic THF cycle enzymes (*DHFR*, *MTHFR*, and *MTHFD1*) and mitochondrial ones (*MTHFD1L*, *MTHFD2*, and *MTHFD2L*) are expressed at high levels in lesional psoriatic plaques, confirming the important role for folate availability in this disease. Psoriatic lesions are characterized by epidermal alterations and a high number of skin-infiltrating immune cells including polarized T helper 1 (T_H1), T_H17 , and T_H22 lymphocytes, which release proinflammatory cytokines such as interferon- γ , IL-17, and IL-22, respectively (35–37). These lymphocyte-released cytokines, together with tumor necrosis factor- α (TNF- α), promote hyperproliferation and impair the terminal differentiation of epidermal keratinocytes, and they induce the secretion of proinflammatory molecules, thus contributing to skin alterations and the manifestation of erythematous plaques (23). Notably, IL-23 cytokine, released by epidermal dendritic cells, plays a central role in psoriasis pathogenesis, by sustaining T_H17

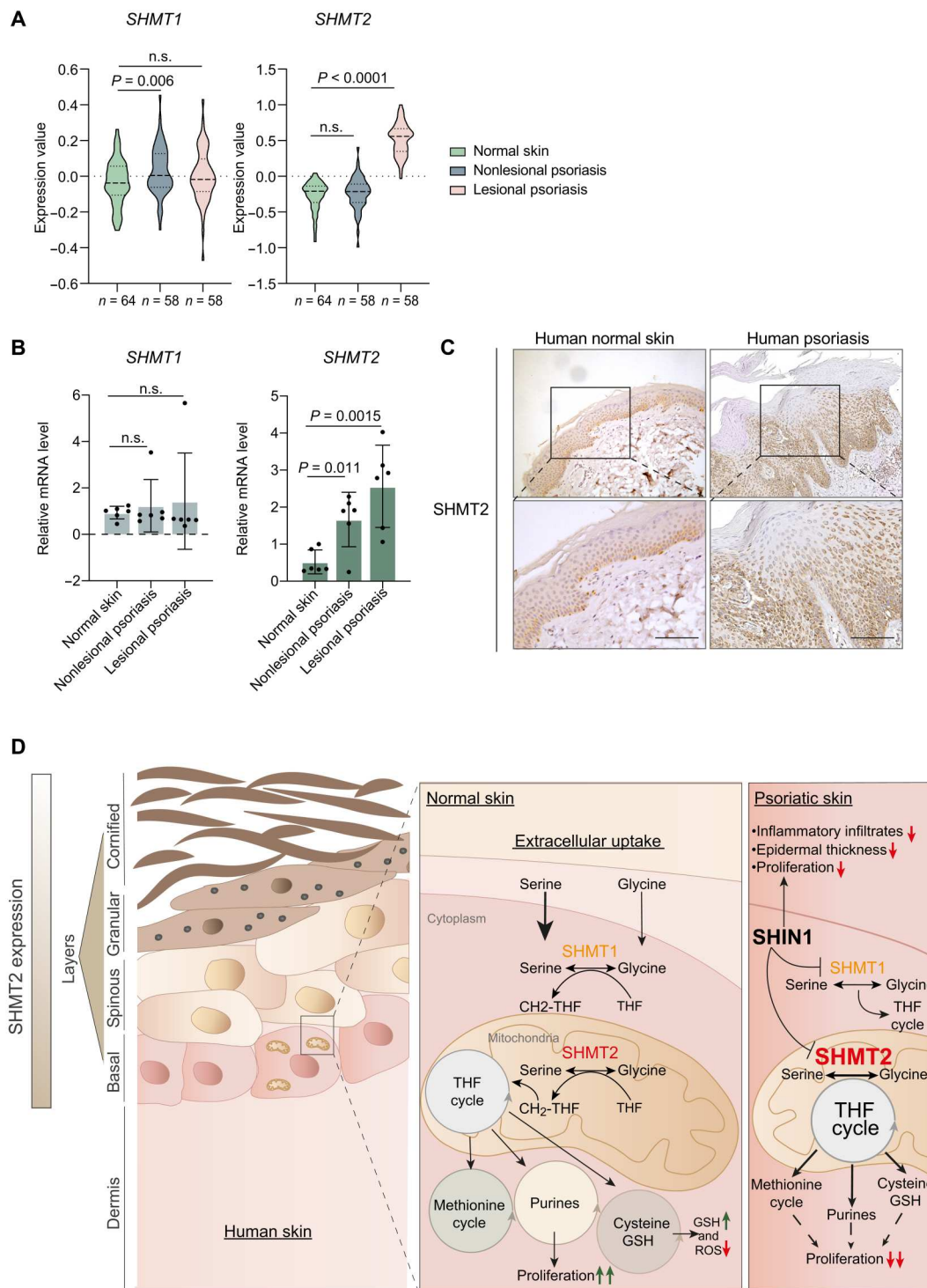


Fig. 8. SHMT2 is overexpressed in human psoriatic lesions. (A) Bioinformatics analysis of *SHMT1* and *SHMT2* expression in the skin of healthy individuals ($n = 64$) and from nonlesional ($n = 54$) and lesional ($n = 54$) areas in the skin of psoriatic patients (GSE13355). (B) RT-qPCR analysis of *SHMT1* and *SHMT2* mRNA was performed with human healthy skin samples ($n = 6$) and nonlesional ($n = 7$) and lesional ($n = 6$) skin of patients affected by plaque-type psoriasis. (C) Immunohistochemistry of SHMT2 in human normal skin ($n = 3$) and human skin affected by psoriasis ($n = 3$). Scale bar, 200 μm . One representative experiment of three is shown. $P < 0.05$. (D) Schematic model of the role of SHMT2 in normal keratinocytes and in psoriasis. Under normal conditions, keratinocytes use extracellular glycine and serine to sustain proliferation. SHMT2 synthesizes glycine and provides one-carbon units for purine and GSH synthesis, thus supporting keratinocyte proliferation and maintaining redox balance. This mechanism is amplified in psoriasis. Topical treatment with SHIN1 inhibitor rebalances keratinocyte proliferation and ameliorates the clinical features associated with psoriasis.

differentiation. Several monoclonal antibodies blocking IL-17 and IL-23 have demonstrated efficacy and safety and are currently approved in the treatment of psoriasis, underscoring the critical role of IL-23/IL-17 signature in psoriasis pathogenesis (38, 39). In particular, biologic treatments anti-IL-17 (i.e., secukinumab and ixekizumab), anti-IL-12/23 (i.e., ustekinumab), anti-IL-23 (i.e., risankizumab and guselkumab), and anti-TNF- α (i.e., adalimumab and etanercept) resulted to be more effective and safer than nonbiological systemic agents, including methotrexate (MTX) and small molecules inhibiting selective cytokine-dependent tyrosine kinases (40). However, although these therapies improve psoriatic symptoms, their effects on long-term disease modification still need to be addressed. In addition, treatments against immunological targets are not completely effective, and several adverse effects have been observed in patients, resulting in immunotherapy interruption, followed by recurrence and chronicity (41–43). Last, when biologic systemic treatments are interrupted, psoriasis plaques invariably reappear, and reduced efficacy is often observed upon retreatment (44). Therefore, for comprehensive management of psoriatic patients, alternative therapeutic approaches are still needed. As a matter of fact, metabolic pathways controlling the activation and differentiation of keratinocytes and immune cells in chronic inflammatory skin diseases and in cutaneous neoplastic disorders represent a valid therapeutic target for future adjunctive interventions. One of the oldest oral pharmacological treatments licensed for psoriasis is MTX, a folic acid analog with antiproliferative, immunosuppressive, and anti-inflammatory properties (45). Mechanistically, MTX inhibits cell proliferation by blocking DNA/RNA synthesis, through the inhibition of the dihydrofolate reductase, necessary for production of pyrimidine and purine nucleotides (46, 47). Although widely used, MTX presents negative side effects, i.e., difficulties in dosage identification and toxicity in high proliferating tissues (i.e., hematopoietic bone marrow cells, epithelial gastrointestinal tube, and epidermal cells).

For comprehensive management of psoriatic patients, alternative therapeutic approaches are still needed. Although SHIN1, a folate-competitive cell-permeable inhibitor of human SHMT1/2 (23) is not selective for SHMT2, the experiments shown represent the proof of concept that inhibition of SHMTs can ameliorate the clinical features associated with psoriasis (Fig. 8D). Because serine metabolism, through SHMT2, fuels keratinocyte proliferation and psoriasis-like symptoms, it is reasonable to hypothesize that targeting serine uptake and/or inhibiting the SHMT2 enzyme may be a promising alternative therapeutic strategy for treatment and long-term management of psoriasis and possibly for other skin diseases characterized by aberrant keratinocyte proliferation and inflammation.

MATERIAL AND METHODS

Cell culture, transfection, proliferation, and clonogenic assays

HEK293T, normal human epidermal keratinocytes (Gibco, catalog no. C-001-5C) and human TERT-immortalized keratinocytes (hTert/Ker-CT, American Type Culture Collection, CRL4048, lot. no. 0213) were cultured in EpiLife medium with the addition of Human Keratinocyte Growth Supplements (HKGS, Life Technologies). Serine and/or glycine starvation experiments were done using minimum essential medium without nonessential amino acids

(Lonza, catalog no. 04-719Q). PHGDH inhibition was done adding 1 μ M CBR-5884 (MedChemExpress, catalog no. HY-100012) to the culture medium. For proliferation analysis, Incucyte Live-Cell Analysis (Essen BioScience) was used. For siRNA-mediated knockdown experiments, 6×10^5 cells were seeded and transfected with specific siRNAs (table S2) using Lipofectamine RNAiMAX transfection reagent (Invitrogen). Cells were collected 72 hours after transfection. A total of 6×10^5 human keratinocytes were seeded and treated with SHIN1 (25 μ M; MedChemExpress, catalog no. HY-112066) and collected 48 hours after treatment. To make rescue experiment, after 12 hours of SHMT2 silencing or SHIN1 treatment, cells were treated with hypoxanthine (100 μ M; Sigma-Aldrich, catalog no. H9636), thymidine (16 μ M; Sigma-Aldrich, catalog no. T9250), formate (1 mM; Sigma-Aldrich, catalog no. 247596), or GSH-reduced ethyl ester (100 μ M; Sigma-Aldrich, catalog no. G1404). HEK293T were differentiated with 1.2 mM CaCl_2 added to culture medium and collected at the following time points: 0, 3, 6, and 9 days. Cells were pulse-labeled with 10 μ M EdU and processed with a Click-iT EdU Alexa Fluor 488 flow cytometry assay kit (Invitrogen, catalog no. C10337). For both EdU assay and propidium iodide (PI), cells were stained and analyzed using a CytoFLEX cytometer (Beckman Coulter). A total of 12,000 events were evaluated for each proliferation analysis. The cell cycle analysis with PI was performed using Kaluza software. Last, for the clonogenicity assay, 100 cells were plated with 1×10^6 NIH 3T3 fibroblasts previously treated with mitomycin C (10 μ g/ml; Sigma-Aldrich). The cells were cultured in 60% (v/v) Dulbecco's modified Eagle's medium, 30% (v/v) Ham F-12, 10% (v/v) fetal bovine serum, adenine (24.3 μ g/ml), insulin (5 μ g/ml), hydrocortisone (0.4 μ g/ml), and 10^{-10} M cholera toxin. Three days after seeding, epidermal growth factor (10 ng/ml) was added. For the clonogenicity assay after SHIN1 treatment, 100 cells were plated with 1×10^6 NIH 3T3 fibroblasts previously treated with mitomycin C (10 μ g/ml; Sigma-Aldrich).

Seahorse flux analysis

The cellular OCR and ECAR were measured using an XF Cell Mito Stress Test kit (Agilent) and an XFe96 extracellular flux analyzer (Seahorse Bioscience, Houston, TX, USA). The sensor cartridge for the XFe analyzer was hydrated in a 37°C incubator without CO_2 a day before the experiment. According to the manufacturer's instructions, the following stressor concentrations were optimized and added: 1 μ M oligomycin as a complex V inhibitor, 0.8 μ M FCCP (an uncoupling agent), and 0.5 μ M rotenone/antimycin A (inhibitors of complexes I and III). OCR was normalized on the basis of total protein per well per 10,000 cells. Each sample/treatment was analyzed in at least eight wells for the experiment, and two independent experiments were performed.

Mitochondria analysis and ROS quantification

HEK293T cells were trypsinized and stained with chloromethyl 2',7'-dichlorodihydrofluorescein diacetate (CM-H₂DCFDA) (10 μ M; Invitrogen), MitoSOX Red (5 μ M; Invitrogen), and JC1 (2 μ M). The cells were incubated for 20 min at 37°C and analyzed by flow cytometry, obtaining 12,000 events per sample. In detail, the CM-H₂DCFDA fluorescence signal was detected in the fluorescein isothiocyanate (FITC) channel, MitoSOX Red was detected in the phycoerythrin (PE) channel, and JC1 fluorescence was detected in both FITC and PE channels.

Metabolite profiling

The metabolites were extracted using cold methanol and chloroform. Then, the tubes were centrifuged at 13,500g for 10 min at 4°C to obtain a pellet. Last, the dried samples were resuspended in 0.1 ml of water and 5% formic acid and transferred onto glass autosampler vials for liquid chromatography–mass spectrometry (LC-MS) analysis. Twenty microliters of supernatant was injected into an ultrahigh-performance LC (UHPLC) system (Ultimate 3000, Thermo Fisher Scientific) and run in positive ion mode. The UHPLC system was coupled online with a Q Exactive mass spectrometer (Thermo Fisher Scientific) scanning in full MS mode (two μ scans) at 70,000 resolutions in the 67 to 1000 mass/charge ratio range and targeting 1×10^6 ions with a maximum ion injection time of 35 ms. Raw files of replicates were exported and converted into mzXML format through MassMatrix (Cleveland, OH) and then processed by MAVEN.52 (available at <http://genomics-pubs.princeton.edu/mzroll/>). Spectrometry chromatograms were assessed for peak alignment, matching and comparing parent and fragment ions, and tentative metabolite identification (within a 2-part per million mass deviation range between observed and expected results based on the imported Kyoto Encyclopedia of Genes and Genomes database). For metabolomic array, cells transfected with specific siRNAs (siSCR; siSHMT2 or siMTHFD1L) or treated with SHIN1 were collected and homogenized with a mixture of Millipore ultrapure water and cold methanol. After centrifugation at 13,500g and 4°C for 10 min, a 30- μ l aliquot of the supernatant was carefully transferred to a 96-well plate for derivatization. The plate was then transferred to a Biomek 4000 workstation (Biomek 4000, Beckman Coulter, Brea, California, USA). Twenty microliters of freshly prepared derivative reagents [200 mM 3-Nitrophenylhydrazine (3-NPH) in 75% aqueous methanol and 96 mM 1-ethyl-3-(3-dimethylaminopropyl)carbodiimide–6% pyridine solution in methanol] were added to each well. The plate was sealed, and the derivatization was carried out at 30°C for 60 min. After derivatization, the plate was lyophilized (Labconco, Kansas City, MO, USA) to dry. Then, 400 μ l of ice-cold 50% methanol solution was added to resolve the sample, followed by 4000g centrifugation at 4°C for 30 min. Supernatant (135 μ l) was transferred to a new 96-well plate in each well. Last, the plate was sealed for LC-MS analysis. The raw data files generated by ultra-performance LC–quadrupole time-of-flight MS (UPLC-QTOF-MS) were processed using the Targeted Metabolome Batch Quantification (TMBQ) software (v1.0, HMI, Shenzhen, Guangdong, China) to perform peak integration, calibration, and quantification for each metabolite.

Intracellular α -ketoglutarate measurement

Cells were collected and pellet was snap-frozen in liquid nitrogen and then stored at -80°C . The α -ketoglutarate was measured by an α -ketoglutarate assay kit (Cell Biolabs, catalog no. MET-5131) following the manufacturer's instructions. Colorimetric signal was read using the Labsystems Multiskan Ascent instrument; the obtained values (two technical replicates per biological replicate) were normalized on total protein extract; $n = 3$ biological replicates has been conducted; the P value was calculated by ordinary one-way analysis of variance (ANOVA) with Tukey's correction.

Isotope labeling and metabolic fluxes

A total of 1.5×10^5 cells were seeded in six-well plates in complete medium and allowed to grow for 48 hours. At the start of the assay, cells were washed with phosphate-buffered saline (PBS) and received the assay medium (without serine or glycine) supplemented with both $^{13}\text{C}_2^{15}\text{N}_1$ -glycine (0.4 mM; Sigma-Aldrich, catalog no. 489522) or $^{13}\text{C}_3^{15}\text{N}_1$ -serine (0.4 mM; Sigma-Aldrich, catalog no. 608130). Two biological replicates of the medium and cell pellet were collected at the time points of 4, 8, 12, 24, and 32 hours after incubation. Cell pellets were homogenized with a mixture of Millipore ultrapure water and cold methanol. After centrifugation at 13,500g and 4°C for 10 min, a 20- μ l aliquot of the supernatant was carefully transferred to a 96-well plate for derivatization. Twenty microliters of working standard solutions, cell extracts, or medium was added to a 96-well plate. Ten microliters of dithiothreitol (DTT) was added into each well, and the reaction solutions were placed on the thermos shaker for 10 min at 55°C and 800 rpm. After short centrifugation, 10 μ l of indole-3-acetic acid was added, followed by heating to 55°C for 10 min at 800 rpm. After short centrifugation, 10 μ l of DTT was added, followed by heating to 55°C for 10 min at 800 rpm. Subsequently, 10 μ l of the supernatant was collected to be derivatized with the AccQTag reagents in the light of the manufacturer's protocol procedure. Last, 5 μ l of the derivative solutions were transferred for UPLC-QTOF-MS analysis. The raw data were processed using the TargetLynx application manager (Waters Corp., Milford, MA) to obtain calibration equations and the measured concentration of each amino acid in the cell and medium samples.

IMQ mouse model of psoriasis

An 8-week-old female BALB/cJ mouse group (Harlan Laboratories, San Pietro al Nativone, Italy) was treated for five consecutive days with 5% (62.5 mg) IMQ (Aldara cream, Meda AB, Solna, Sweden) ($n = 6$). An 8-week-old female group was treated for five consecutive days with 5% (62.5 mg) IMQ with the addition of SHIN1 (MedChemExpress, catalog no. HY-112066) starting on the third day of treatment (1 mM) ($n = 6$). Treatments with vehicle [dimethyl sulfoxide (DMSO)] (control group, $n = 2$) or SHIN1 administered alone started on day 0 of IMQ administration. On day 5, full-thickness skin biopsy samples of the treated area were collected with an 8-mm biopsy puncher. Skin was either snap-frozen in liquid N_2 for total RNA preparation or fixed in neutral buffered formalin (Sigma-Aldrich, St. Louis, MO, USA) for histopathological and immunohistochemistry analyses. Each complete experiment was repeated twice with similar results. All mouse procedures were carried out in accordance with institutional standard guidelines. The experimental design was authorized by the Italian Health Minister (protocol no. 112/2021-PR).

Histological and immunohistochemistry analyses

Formalin-fixed paraffin-embedded (FFPE) sections (5 μm) of human normal and psoriatic skin were dewaxed for 2 hours at 60°C, treated with Bio Clear (BIO-OPTICA), and rehydrated with alcohol scale and double-distilled H_2O . Immunohistochemical staining was performed using UltraTek HRP antipolyvalent [diaminobenzidine (DAB)] (ScyTek Laboratories, catalog no. AMF080). Samples were boiled at 95°C for 10 min in sodium citrate buffer at pH 6.0 for antigen retrieval. Anti-SHMT2 antibody was incubated (1:100; Sigma-Aldrich, catalog no. HPA020549) for 1 hour.

Sections were counterstained with Mayer's haematoxylin (BIO-OPTICA), dehydrated, and mounted using Bio Mount HM (BIO-OPTICA). All the tissues were obtained from adult donors. The samples were used in this study with the approval of the institutional review board of the Istituto Dermopatico dell'Immacolata (IDI-IRCCS) before the acquisition of informed patient consent (n.41/CE/2020; 656/1). Tissue sections from murine FFPE skin biopsy samples were deparaffinized and stained with H&E for histological analysis. Epidermal and scale thickness and cell infiltrate number were analyzed as parameters of skin acanthosis and inflammation. Average epidermal and scale thicknesses were quantified by a researcher blind to the experimental groups who took five measurements in three sections of each mouse. Cells infiltrating the dermis were also counted in three skin sections in each mouse. Immunohistochemistry was performed with primary antibodies against Ki67 (1:250; Novocastra, catalog no. NCLk67P), CD3 (1:100; Dako, catalog no. A0452), LY6G (1:30; Pharmingen, catalog no. 550291), or K10 (1:1000; Covance, catalog no. PRB-159P). For antigen retrieval, samples were boiled in Dako buffer (catalog no. S1700) at 96°C for 25 min for Ki67, in proteinase K (Dako) for 10 min for LY6G and CD3, and in sodium citrate buffer (pH 6.0) at 96°C for 10 min for K10. Sections were counterstained with Mayer's haematoxylin and were visually analyzed by two pathologists experienced in dermatology. Positivity was evaluated in five adjacent fields at a magnification of $\times 200$.

Immunoblotting

In vitro differentiated keratinocytes were lysed with SDS lysis buffer [100 mM tris (pH 8.8), 1% SDS, 5 mM EDTA, 20 mM DTT, and 2 mM of 4-[2-Aminoethyl] benzenesulfonyl fluoride hydrochloride (AESBF)]. Human epidermal keratinocytes used for silencing and SHIN1 treatment were collected and lysed in radioimmunoprecipitation assay buffer [50 mM tris-Cl (pH 7.4), 150 mM NaCl, 1% NP-40, 0.25% Na-deoxycholate, 1 mM AESBF, and 1 mM DTT]. Total protein extracts (20 to 50 μ g) were separated using SDS polyacrylamide gels. The following antibodies were used: anti-SHMT1 (1:300; Sigma-Aldrich, catalog no. HPA023314), anti-SHMT2 (1:500; Sigma-Aldrich, catalog no. HPA020549), anti-K10 (1:1000; Covance, catalog no. PRB-159P), anti-glyceraldehyde-3-phosphate dehydrogenase (GAPDH) (1:15,000; Sigma-Aldrich, catalog no. G8795), anti-p63- α (1:500; Cell Signaling Technology, catalog no. 13109) and anti-OXPPOS cocktail (1:250; MitoSciences), anti-loricrin (BioLegend, catalog no. 905104), anti-MTHFD1L (Proteintech, catalog no.16113-1-AP), anti-H3K27me3 (Millipore, catalog no. 07-449), and anti-H3 (Abcam, catalog no. Ab10799). Uncropped images of the Western blots are shown in fig. S7.

Immunofluorescence

After seeding on slides sterilized with methanol, HEK cells were fixed for 10 min in 10% formalin-buffered solution and permeabilized for 10 min in 0.2% Triton X-100/PBS. The following antibodies were used: anti-SHMT1 (1:300; Sigma-Aldrich, catalog no. HPA023314), anti-SHMT2 (1:500; Sigma-Aldrich, catalog no. HPA020549), and anti-cyclophilin D (MitoSciences, catalog no. MSA04). The following secondary antibodies were used: anti-rabbit Alexa Fluor 488- or Alexa Fluor 568-conjugated antibodies (1:1000; Invitrogen) together with 4',6-diamidino-2-phenylindole (1 μ g/ml; Sigma-Aldrich) for nuclear DNA staining. For cytoskeleton staining, Alexa Fluor 488-conjugated phalloidin was added to

the secondary antibody solution (1:1000; Thermo Fisher Scientific). Samples were analyzed by confocal laser microscopy (NIKON Eclipse Ti) using EZ C.1 software (Nikon).

RNA extraction and RT-qPCR

HEK cells were lysed in RNeasy Lysis Buffer (RLT) (QIAGEN). Total RNA was isolated using the RNeasy Mini Kit (QIAGEN). Total RNA was quantified using a NanoDrop spectrophotometer (Thermo Fisher Scientific). Total RNA was used for complementary DNA (cDNA) synthesis with a SensiFAST cDNA synthesis kit (Bioline). With RNA extracted from mouse skin, SuperScript VILO (Invitrogen, catalog no. 11754050) was used for cDNA synthesis. qPCR was performed with a GoTaq Real-Time PCR System (Promega) in an Applied Biosystems 7500 Real-Time 15 PCR System (Applied Biosystems) using appropriate qPCR primers (table S3). TATA box-binding protein (*TBP*) and Beta-2-Microglobulin (*B2M*) were used as housekeeping genes for data normalization. The expression of each gene was defined by the threshold cycle (C_t), and relative expression levels were calculated by using the $2^{-\Delta\Delta C_t}$ method.

Statistical analysis

Student's *t* test was used for statistical analysis, one-way ANOVA followed by Bonferroni post hoc comparison test was used for the seahorse analysis, and one-way ANOVA was used for growth curves. $P < 0.05$ and $P < 0.01$ were considered statistically significant.

Bioinformatics analysis and data availability statement

Analysis of *SHMT1* and *SHMT2* expression was performed using high-throughput data performed on human proliferative keratinocytes and available from Encyclopedia of DNA Elements (ENCODE) at University of California, Santa Cruz (UCSC) (<https://genome.ucsc.edu/ENCODE/>) and ENCODE project (www.encodeproject.org/). For *SHMT1* and *SHMT2* expression analysis, in vitro differentiated keratinocyte RNA-seq data were obtained from undifferentiated keratinocyte and keratinocyte treated with calcium chloride and allowed to differentiate for 3 or 6 days (ENCSR527SSD, ENCSR959LTT, and ENCSR034RPU). For CAGE sequencing of *SHMT1* and *SHMT2* data available on ENCODE at UCSC were analyzed (GSM8493679). For analysis of gene expression at the mRNA level of the different genes involved in one-carbon metabolism in normal skin and lesional and nonlesional psoriatic skin, public databases available through GEO datasets (www.ncbi.nlm.nih.gov/gds) were analyzed (GSE13355). All data needed to evaluate the conclusions in the paper are present in the paper and/or the Supplementary Materials.

Supplementary Materials

This PDF file includes:

Figs. S1 to S7

Tables S2 and S3

Other Supplementary Material for this manuscript includes the following:

Table S1

[View/request a protocol for this paper from Bio-protocol.](#)

REFERENCES AND NOTES

- E. Candi, R. Schmidt, G. Melino, The cornified envelope: A model of cell death in the skin. *Nat. Rev. Mol. Cell Biol.* **6**, 328–340 (2005).
- C. Blanpain, E. Fuchs, Epidermal stem cells of the skin. *Annu. Rev. Cell Dev. Biol.* **22**, 339–373 (2006).
- S. C. Baksh, P. K. Todorova, S. Gur-Cohen, B. Hurwitz, Y. Ge, J. S. S. Novak, M. T. Tierney, J. dela Cruz-Racelis, E. Fuchs, L. W. S. Finley, Extracellular serine controls epidermal stem cell fate and tumour initiation. *Nat. Cell Biol.* **22**, 1396 (2020).
- J. S. S. Novak, S. C. Baksh, E. Fuchs, Dietary interventions as regulators of stem cell behavior in homeostasis and disease. *Genes Dev.* **35**, 199–211 (2021).
- G. Viticchiè, M. Agostini, A. M. Lena, M. Mancini, H. Zhou, L. Zolla, D. Dinsdale, G. Saintigny, G. Melino, E. Candi, P63 supports aerobic respiration through hexokinase II. *Proc. Natl. Acad. Sci. U.S.A.* **112**, 11577–11582 (2015).
- B. W. Carey, L. W. S. Finley, J. R. Cross, C. D. Allis, C. B. Thompson, Intracellular α -ketoglutarate maintains the pluripotency of embryonic stem cells. *Nature* **518**, 413–416 (2015).
- A. Flores, J. Schell, A. S. Krall, D. Jelinek, M. Miranda, M. Grigorian, D. Braas, A. C. White, J. L. Zhou, N. A. Graham, T. Graeber, P. Seth, D. Evsenko, H. A. Collier, J. Rutter, H. R. Christofk, W. E. Lowry, Lactate dehydrogenase activity drives hair follicle stem cell activation. *Nat. Cell Biol.* **19**, 1017–1026 (2017).
- C. F. Labuschagne, N. J. F. van den Broek, G. M. Mackay, K. H. Vousden, O. D. K. Maddocks, Serine, but not glycine, supports one-carbon metabolism and proliferation of cancer cells. *Cell Rep.* **7**, 1248–1258 (2014).
- T. W. M. Fan, R. C. Bruntz, Y. Yang, H. Song, Y. Chernyavskaya, P. Deng, Y. Zhang, P. P. Shah, L. J. Beverly, Z. Qi, A. L. Mahan, R. M. Higashi, C. V. Dang, A. N. Lane, De novo synthesis of serine and glycine fuels purine nucleotide biosynthesis in human lung cancer tissues. *J. Biol. Chem.* **294**, 13464–13477 (2019).
- R. Possemato, K. M. Marks, Y. D. Shaul, M. E. Pacold, D. Kim, K. Birsoy, S. Sethumadhavan, H.-K. Woo, H. G. Jang, A. K. Jha, W. W. Chen, F. G. Barrett, N. Stransky, Z.-Y. Tsun, G. S. Cowley, J. Barretina, N. Y. Kalaany, P. P. Hsu, K. Ottina, A. M. Chan, B. Yuan, L. A. Garraway, D. E. Root, M. Mino-Kenudson, E. F. Brachtel, E. M. Driggers, D. M. Sabatini, Functional genomics reveal that the serine synthesis pathway is essential in breast cancer. *Nature* **476**, 346–350 (2011).
- S. R. Davis, P. W. Stacpoole, J. Williamson, L. S. Kick, E. P. Quinlivan, B. S. Coats, B. Shane, L. B. Bailey, J. F. Gregory III, Tracer-derived total and folate-dependent homocysteine remethylation and synthesis rates in humans indicate that serine is the main one-carbon donor. *Am. J. Physiol. Endocrinol. Metab.* **286**, E272–E279 (2004).
- A. C. Newman, O. D. K. Maddocks, Serine and functional metabolites in cancer. *Trends Cell Biol.* **27**, 645–657 (2017).
- I. Amelio, F. Cutruzzolà, A. Antonov, M. Agostini, G. Melino, Serine and glycine metabolism in cancer. *Trends Biochem. Sci.* **39**, 191–198 (2014).
- G. Giardina, A. Paone, A. Tramonti, R. Lucchi, M. Marani, M. C. Magnifico, A. Bouzidi, V. Pontecorvi, G. Guiducci, C. Zamparelli, S. Rinaldo, A. Paiardini, R. Contestabile, F. Cutruzzolà, The catalytic activity of serine hydroxymethyltransferase is essential for de novo nuclear dTMP synthesis in lung cancer cells. *FEBS J.* **285**, 3238–3253 (2018).
- A. Paiardini, A. Tramonti, D. Schirch, G. Guiducci, M. L. di Salvo, A. Fiascarelli, A. Giorgi, B. Maras, F. Cutruzzolà, R. Contestabile, Differential 3-bromopyruvate inhibition of cytosolic and mitochondrial human serine hydroxymethyltransferase isoforms, key enzymes in cancer metabolic reprogramming. *Biochim. Biophys.* **1864**, 1506–1517 (2016).
- D. D. Anderson, J. Y. Eoms, P. J. Stovers, Competition between sumoylation and ubiquitination of serine hydroxymethyltransferase 1 determines its nuclear localization and its accumulation in the nucleus. *J. Biol. Chem.* **287**, 4790–4799 (2012).
- A. M. Intlekofer, L. W. S. Finley, Metabolic signatures of cancer cells and stem cells. *Nat. Metab.* **1**, 177–188 (2019).
- O. D. K. Maddocks, C. R. Berkers, S. M. Mason, L. Zheng, K. Blyth, E. Gottlieb, K. H. Vousden, Serine starvation induces stress and p53-dependent metabolic remodelling in cancer cells. *Nature* **493**, 542–546 (2013).
- E. H. Ma, G. Bantug, T. Griss, S. Condotta, R. M. Johnson, B. Samborska, N. Mainolfi, V. Suri, H. Guak, M. L. Balmer, M. J. Verway, T. C. Raissi, H. Tsui, G. Boukhaled, S. Henriques da Costa, C. Frezza, C. M. Krawczyk, A. Friedman, M. Manfredi, M. J. Richer, C. Hess, R. G. Jones, Serine is an essential metabolite for effector T cell expansion. *Cell Metab.* **25**, 345–357 (2017).
- J. W. Locasale, A. R. Grassian, T. Melman, C. A. Lyssiotis, K. R. Mattaini, A. J. Bass, G. Heffron, C. M. Metallo, T. Muranen, H. Sharf, A. T. Sasaki, D. Anastasiou, E. Mullarky, N. I. Vokes, M. Sasaki, R. Beroukhim, G. Stephanopoulos, A. H. Ligon, M. Meyerson, A. L. Richardson, L. Chin, G. Wagner, J. M. Asara, J. S. Brugge, L. C. Cantley, M. G. Vander Heiden, Phosphoglycerate dehydrogenase diverts glycolytic flux and contributes to oncogenesis. *Nat. Gen.* **43**, 869–874 (2011).
- J. W. Locasale, Serine, glycine and one-carbon units: Cancer metabolism in full circle. *Nat. Rev. Cancer* **13**, 572–583 (2013).
- M. Jain, R. Nilsson, S. Sharma, N. Madhusudhan, T. Kitami, A. L. Souza, R. Kafri, M. W. Kirschner, C. B. Clish, V. K. Mootha, Metabolite profiling identifies a key role for glycine in rapid cancer cell proliferation. *Science* **336**, 1040–1044 (2012).
- G. S. Ducker, J. M. Ghergurovich, N. Mainolfi, V. Suri, S. K. Jeong, S. H. J. Li, A. Friedman, M. G. Manfredi, Z. Gitai, H. Kim, J. D. Rabinowitz, Human SHMT inhibitors reveal defective glycine import as a targetable metabolic vulnerability of diffuse large B-cell lymphoma. *Proc. Natl. Acad. Sci. U.S.A.* **114**, 11404–11409 (2017).
- R. J. Morscher, G. S. Ducker, S. H.-J. Li, J. A. Mayer, Z. Gitai, W. Sperl, J. D. Rabinowitz, Mitochondrial translation requires folate-dependent tRNA methylation. *Nature* **554**, 128–132 (2018).
- D. R. Minton, M. Nam, D. J. McLaughlin, J. Shin, E. C. Bayraktar, S. W. Alvarez, V. O. Sviderskiy, T. Papagiannakopoulos, D. M. Sabatini, K. Birsoy, R. Possemato, Serine catabolism by SHMT2 is required for proper mitochondrial translation initiation and maintenance of formylmethionyl-tRNAs. *Mol. Cell* **69**, 610–621.e5 (2018).
- M. Lowes, A. Bowcock, J. Krueger, Pathogenesis and therapy of psoriasis. *Nature* **445**, 866–873 (2007).
- P. Bielecki, S. Riesenfeld, J. Hütter, E. Torlai Triglia, M. Kowalczyk, R. Ricardo-Gonzalez, M. Lian, M. Amezua Vesely, L. Kroehling, H. Xu, M. Slyper, C. Muus, Ludwig LS, E. Christian, L. Tao, A. Kedaigle, H. Steach, A. York, M. Skadow, P. Yaghoubi, D. Dionne, A. Jarret, H. McGee, C. Porter, P. Licona-Limón, W. Bailis, R. Jackson, N. Gagliani, G. Gasteiger, R. Locksley, A. Regev, R. Flavell, Skin-resident innate lymphoid cells converge on a pathogenic effector state. *Nature* **592**, 128–132 (2021).
- K. Ghoreschi, A. Balato, C. Enerbäck, R. Sabat, Therapeutics targeting the IL-23 and IL-17 pathway in psoriasis. *Lancet* **397**, 754–766 (2021).
- L. van der Fits, S. Mourits, J. S. A. Voerman, M. Kant, L. Boon, J. D. Laman, F. Cornelissen, A.-M. Mus, E. Florencia, E. P. Prens, E. Lubberts, Imiquimod-induced psoriasis-like skin inflammation in mice is mediated via the IL-23/IL-17 axis. *J. Immunol.* **182**, 5836–5845 (2009).
- A. B. van Belle, M. de Heusch, M. M. Lemaire, E. Hendrickx, G. Warnier, K. Dunussi-Joannopoulos, L. A. Fouser, J.-C. Renaud, L. Dumoutier, IL-22 is required for imiquimod-induced psoriasiform skin inflammation in mice. *J. Immunol.* **188**, 462–469 (2012).
- M. Morelli, C. Scarponi, L. Mercurio, F. Facchiano, S. Pallotta, S. Madonna, G. Girolomoni, C. Albanesi, Selective immunomodulation of inflammatory pathways in keratinocytes by the Janus kinase (JAK) inhibitor tofacitinib: Implications for the employment of JAK-targeting drugs in psoriasis. *J. Immunol. Res.* **2018**, 7897263 (2018).
- W. H. Boehncke, M. P. Schön, *Lancet* **386**, 983–994 (2015).
- E. Wagner, H. Schonhaler, J. Guinea-Viniegra, E. Tschachler, Psoriasis: What we have learned from mouse models. *Nat. Rev. Rheumatol.* **6**, 704–714 (2010).
- Z. Zhang, Z. Zi, E. E. Lee, J. Zhao, D. C. Contreras, A. P. South, E. D. Abel, B. F. Chong, T. Vandergriff, G. A. Hosler, P. E. Scherer, M. Mettlen, J. C. Rathmell, R. J. DeBerardinis, R. C. Wang, Differential glucose requirement in skin homeostasis and injury identifies a therapeutic target for psoriasis. *Nat. Med.* **24**, 617–627 (2018).
- N. Gago-Lopez, L. F. Mellor, D. Megias, G. Martín-Serrano, A. Izeta, F. Jimenez, E. F. Wagner, Role of bulge epidermal stem cells and TSLP signaling in psoriasis. *EMBO Mol. Med.* **11**, e10697 (2019).
- I. McKay, I. Leigh, Altered keratinocyte growth and differentiation in psoriasis. *Clin. Dermatol.* **13**, 105–114 (1995).
- F. Truzzi, A. Marconi, P. Atzei, M. Panza, R. Lotti, K. Dallaglio, R. Tiberio, E. Palazzo, C. Vaschieri, C. Pincelli, p75 neurotrophin receptor mediates apoptosis in transit-amplifying cells and its overexpression restores cell death in psoriatic keratinocytes. *Cell Death Differ.* **18**, 948–958 (2011).
- L. Puig, The role of IL 23 in the treatment of psoriasis. *Expert Rev. Clin. Immunol.* **13**, 525–534 (2017).
- C. Y. Erichsen, P. Jensen, K. Kofoed, Biologic therapies targeting the interleukin (IL)-23/IL-17 immune axis for the treatment of moderate-to-severe plaque psoriasis: A systematic review and meta-analysis. *J. Eur. Acad. Dermatol. Venereol.* **34**, 30–38 (2020).
- E. Sbidian, A. Chaimani, I. Garcia-Doval, G. Do, C. Hua, C. Mazaud, C. Droitcourt, C. Hughes, J. R. Ingram, L. Naldi, O. Chosidow, L. le Cleach, Systemic pharmacological treatments for chronic plaque psoriasis: A network meta-analysis. *Cochrane Database Syst. Rev.* **12**, CD011535 (2017).
- A. Baylet, M. Laclaverie, L. Marchand, S. Bordes, B. Closs-Gonthier, L. Delpy, Immunotherapies in cutaneous pathologies: An overview. *Drug Discov. Today* **26**, 248–255 (2021).
- J. A. Bridge, J. C. Lee, A. Daud, J. W. Wells, J. A. Bluestone, Cytokines, chemokines, and other biomarkers of response for checkpoint inhibitor therapy in skin cancer. *Front. Med. (Lansanne)* **5**, 351 (2018).
- U. Blume-Peytavi, M. Bagot, D. Tennstedt, M. S. Aroman, E. Stockfleth, A. Zlotogorski, V. Megeaudo, A. M. Schmitt, C. Paul, H. W. Lim, V. Georgescu, B. Dréno, T. Nocera, Dermatology today and tomorrow: From symptom control to targeted therapy. *J. Eur. Acad. Dermatol. Venereol.* **33Suppl 1**, 3–36 (2019).

44. U. Mrowietz, C. L. Leonardi, G. Girolomoni, D. Toth, A. Morita, S. A. Balki, J. C. Szepietowski, P. Regnault, H. Thurston, C. Papavassilis; SCULPTURE Study Group, Secukinumab retreatment-as-needed versus fixed-interval maintenance regimen for moderate to severe plaque psoriasis: A randomized, double-blind, noninferiority trial (SCULPTURE). *J. Am. Acad. Dermatol.* **73**, 27–36.e1 (2015).
45. C. A. Bangert, M. I. Costner, Methotrexate in dermatology. *Dermatol. Ther.* **20**, 216–228 (2007).
46. A. M. Alqarni, M. P. Zeidler, How does methotrexate work? *Biochem. Soc. Trans.* **48**, 559–567 (2020).
47. R.-I. Nedelcu, M. Balaban, G. Turcu, A. Brinzea, D. Ion, M. Antohe, A. Hodoroagea, A. Calinescu, A. Badarau, C. G. Popp, M. Cioplea, L. Nichita, S. Popescu, C. Diaconu, C. Bleotu, D. Pirici, R. Popescu, C. M. Popescu, S. A. Zurac, Efficacy of methotrexate as anti-inflammatory and anti-proliferative drug in dermatology: Three case reports. *Exp. Ther. Med.* **18**, 905–910 (2019).

Acknowledgments: We thank M. Agostini and A. M. Lena for discussion and support, A. Smirnov for help in bioinformatic analysis, M. Montanaro for technical assistance in immunohistochemistry processing, and F. Calavaro for support in metabolic array statistical analysis. **Funding:** This work was mainly supported by Ministry of Health and IDI-IRCCS, grant RF-2019-12368888 (to E.C.), by LazioInnova, grant A0375-2020-36568 UTV-IDI (to E.C.), and

funding from PNRR-PE6 (Heal Italy). The Associazione Italiana Ricerca sul Cancro (AIRC) under IG 2019-ID.23125 project-PI FC, IG 2016-ID.19225-PI EC and the Sapienza University of Rome (for the HYP-ACB Seahorse GA116154C8A94E3D to F.C.) are also acknowledged. **Author contributions:** E.C. designed the research. A.C. performed most of the experiments done on human keratinocytes, RT-qPCR, Western blots, and bioinformatic analysis of datasets. S.R., A.P., and F.C. performed seahorse experiments and analyzed the data. M.M. and A.Z. performed the small-molecule rescue experiments. E.P. performed H3K27me3 and α -ketoglutarate evaluation. S.M., C.S., and C.A. performed the IMQ-mouse model experiments and RT-qPCRs and analyzed the data. A.B. and L.Z. performed metabolomic experiments. L.W. performed stable isotope labeling, metabolic fluxes, and metabolic array. W.J. analyzed the metabolic fluxes and metabolic array and discussed the data. S.P. recruited the psoriatic patients. M.A.-P. analyzed the datasets. E.C., G.M., and F.C. discussed and analyzed the data. E.C. wrote the paper. **Competing interests:** The authors declare that they have no competing interests. **Data and materials availability:** All data needed to evaluate the conclusions in the paper are present in the paper and/or in the Supplementary Materials.

Submitted 12 October 2021
Accepted 16 November 2022
Published 16 December 2022
10.1126/sciadv.abm7902

Extracellular serine empowers epidermal proliferation and psoriasis-like symptoms

Angela Cappello, Mara Mancini, Stefania Madonna, Serena Rinaldo, Alessio Paone, Claudia Scarponi, Antonio Belardo, Lello Zolla, Alessandro Zuccotti, Emanuele Panatta, Sabatino Pallotta, Margherita Annicchiarico-Petruzzelli, Cristina Albanesi, Francesca Cutruzzol, Lu Wang, Wei Jia, Gerry Melino, and Eleonora Candi

Sci. Adv., **8** (50), eabm7902.
DOI: 10.1126/sciadv.abm7902

View the article online

<https://www.science.org/doi/10.1126/sciadv.abm7902>

Permissions

<https://www.science.org/help/reprints-and-permissions>

Use of this article is subject to the [Terms of service](#)

Science Advances (ISSN) is published by the American Association for the Advancement of Science. 1200 New York Avenue NW, Washington, DC 20005. The title *Science Advances* is a registered trademark of AAAS.
Copyright © 2022 The Authors, some rights reserved; exclusive licensee American Association for the Advancement of Science. No claim to original U.S. Government Works. Distributed under a Creative Commons Attribution NonCommercial License 4.0 (CC BY-NC).